Journal of Asian Earth Sciences 111 (2015) 54–71

Contents lists available at ScienceDirect

Journal of Asian Earth Sciences

journal homepage: www.elsevier.com/locate/jseaes

U–Pb zircon geochronology, petrochemical and Sr–Nd isotopic characteristic of Late Neoproterozoic granitoid of the Bornaward Complex (Bardaskan-NE Iran)

R. Monazzami Bagherzadeh [a,*], M.H. Karimpour [a], G. Lang Farmer [b], C.R. Stern [b], J.F. Santos [c], B. Rahimi [a], M.R. Heidarian Shahri [a]

[a] Department of Geology, Ferdowsi University of Mashhad, Islamic Republic of Iran
[b] Department of Geological Sciences, University of Colorado, USA
[c] Department of Geosciences, University of Aveiro, Aveiro, Portugal

ARTICLE INFO

Article history:
Received 3 April 2014
Received in revised form 27 April 2015
Accepted 28 May 2015
Available online 8 June 2015

Keywords:
Taknar
Bornaward
U–Pb dating
Zircon
Sr–Nd
Late Neoproterozoic

ABSTRACT

The Bornaward Granitoid Complex (BGC) in the Taknar Zone is located in the northeast of Central Iranian Block. The BGC consists of granite, alkaligranite, syenogranite, leucogranite, granophyre, monzogranite, granodiorite, tonalite and diorite that have intruded into the center of Taknar Zone. These intrusive rocks affected by low grade metamorphism. Because of there are no reliable isotope dating data, for the Bornaward Granitoid Complex rocks have been proposed discordant ages (Jurassic, Cretaceous or even younger ages) by many studies. In the present study, new isotopic information based on zircon U–Pb dating has revealed the origin and time of the formation of the BGC. These new results do not confirm previously proposed ages. The results obtained from zircon U–Pb dating of the BGC rocks suggest late-Neoproterozoic (Precambrian) age (540–550 Ma). The Bornaward Granitoid Complex is middle-high metaluminous to lower-middle peraluminous and belongs to tholeiite, calc-alkaline to high-K calc-alkaline rock series with enrichment in LIL (Cs, Rb and Ba, U, K, Zr, Y, Th) and depletion in HIL (Sr and Nb, Ta, Ti) elements. Chondrite-normalized Rare Earth Elements (REE) plots indicate minor enrichment of LREE compared to HREE, and strong negative anomaly of Eu compared to other Rare Earth Elements. Furthermore, initial $^{87}Sr/^{86}Sr$ and $^{143}Nd/^{144}Nd$ range from 0.70351 to 0.71689 and 0.511585 to 0.512061, respectively, and initial εNd isotope values for granite, granodiorite and diorite range from −6.73 to 2.52. These all indicate that the BGC has derived from partial melting of distinct basement source regions with very high initial $^{87}Sr/^{86}Sr$ and undergoing extensive crustal contamination (S-type granite).

1. Introduction

The geology of Central and Eastern Iranian terrains is immensely complicated because of the collision between the micro-continents and overprinting of many metamorphic and tectonic events (Stöcklin and Nabavi, 1972) as a result of continuous continental deformation in response to the ongoing convergence between the Arabian (Gondwana) and Turan (Eurasian) plates. However, the overall uniformity of Late Neoproterozoic and Paleozoic platform strata that covered the Zagros, the Central Iran and the Main Alborz provinces led to the predominant notion that all of these regions were once part of the undivided Paleozoic Arabian–Iranian platform of the Gondwanaland supercontinent (Stöcklin, 1968, 1974; Crawford, 1972). Nevertheless, neither the sparse Rb–Sr isochron data from the Central Iranian crystalline rocks (Crawford, 1977) nor the Pb–Pb isochron ages of lead ore bodies in the Central Iran (Huckriede et al., 1962) provided conclusive evidence for the presence of a Precambrian crust in this region. The absence of reliable isotope ages has further complicated interpretation of tectonic setting of other volcanic and granitic rocks. However, the study of Iranian geology has entered a new phase in the past decade. Recently, researchers (e.g., Hassanipak and Ghazi, 2000; Masoudi et al., 2002; Khalatbari-Jafari et al., 2003;

* Corresponding author. Tel.: +98 5138218146, mobile: +98 9155011318; fax: +98 5138212402.
E-mail addresses: rmonazzami@yahoo.com (R.M. Bagherzadeh), mhkarimpour@yahoo.com (M.H. Karimpour), Lang.Farmer@Colorado.EDU (G.L. Farmer), Charles.Stern@Colorado.EDU (C.R. Stern), Jfsantos@ua.pt (J.F. Santos), B_rahimi2000@Yahoo.com (B. Rahimi), Hshahri@Ferdowsi.um.ac.ir (M.R. Heidarian Shahri).

http://dx.doi.org/10.1016/j.jseaes.2015.05.019
1367-9120/

Hassanzadeh et al., 2008; Ghalamghash et al., 2009; Karimpour et al., 2010) have reported new isotope ages (e.g., Rb–Sr, Sm–Nd, U–Pb, K–Ar and Ar–Ar ages) for the Iran igneous rocks.

The Central Iranian terrain consists, from east to west, of three major crustal domains: the Lut Block, the Tabas Block and the Yazd Block (Alavi, 1991). These blocks are separated by a series of intersecting regional-scale faults (Fig. 1).

This research and data rendered the true age and origin of the continental crust in Central Iran, a matter of debate for nearly four decades. We report here the first high-precision U–Pb concordia ages and major and trace elements data, from the magmatic rocks of Late Neoproterozoic Era (Ediacaran period) of the Bornaward Granitoid and volcanic rocks (metarhyolite to metarhyodacite) from the Taknar zone in eastern part of the Central Iran. The study area is located in northeast of Iran (Khorasan Razavi Province), about 280 km southwest of the city of Mashhad and 28 km northwest of Bardaskan (Fig. 1). The Taknar Zone consists of Precambrian, Paleozoic, Mesozoic and Tertiary rocks (Bardaskan geological map 1:100,000). The Taknar zone is an exotic block bordered by two major faults, the Great Kavir Fault (Darouneh) in the south and the Taknar (Rivash) Fault in the north (Fig. 1).

2. Geology

The present study is concerned with granitoid occurrences in the northeastern part of Central Iranian Microcontinental (CIM) in an area named "Taknar zone". The Taknar Inlier near Kashmar, Khorasan Province (NE-Iran), consists of an uplifted portion of the Central Iranian Precambrian to Paleozoic basement and its Mesozoic–Cenozoic cover (Fig. 1). To the south, it is bordered by the Great Kavir Fault (Darouneh Fault), and to the north by the

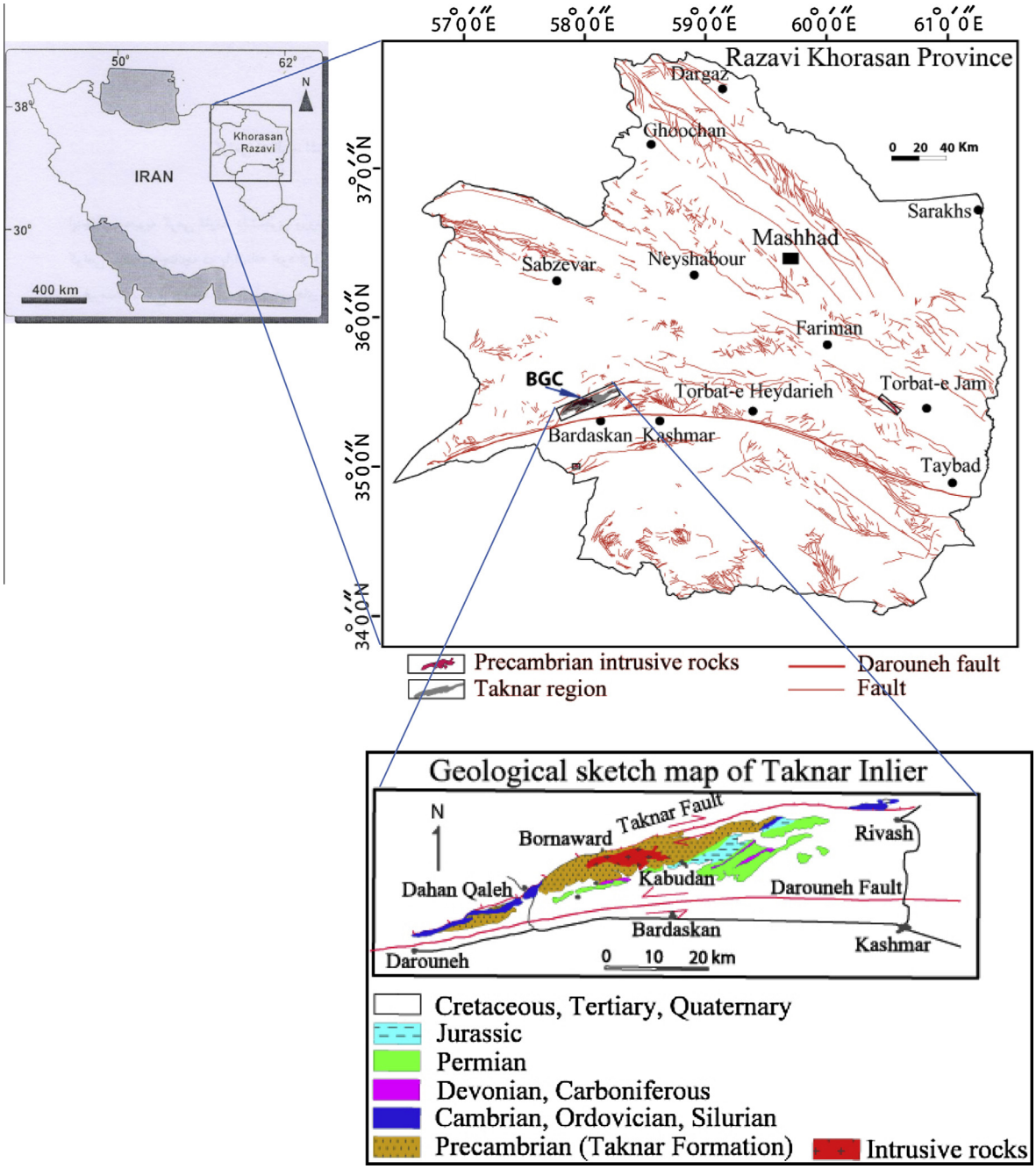

Fig. 1. Location of the Bornaward region and Precambrian intrusive rocks in NE Iran.

Taknar Fault. Along the still recently active sinistral strike-slip fault of the Great Kavir system the Taknar uplift is in direct contact with the northern part of Lut Block. The Taknar uplift is suggested to originally represent a marginal segment of the continental Central and East Iranian Microplate (Fig. 2).

In the central part of Taknar Inlier, the Precambrian volcanic and volcano-sedimentary rocks have been intruded by granites and diorites (Fig. 1). The Precambrian and Paleozoic volcanic and sedimentary rocks have been affected by a low grade metamorphism of pre-Jurassic (Muller and Walter, 1983). The compressional deformation of the Precambrian and Paleozoic Taknar Inlier belongs to Early Cimmerian. Later tectonic events in Late Cretaceous and Cenozoic have caused its uplift. The Taknar Inlier represents the most outcrop of a Central and East-Iranian continental microplate (Muller and Walter, 1983).

The greater part of Taknar Inlier is mainly comprised of Precambrian rhyolites and tuffs with intercalations of sandstone and dolomite in their upper part (Taknar Formation). These rocks have been affected by a low-grade metamorphism. They have been intruded by a granite and diorite complex in their central part (Muller and Walter, 1983).

The lithological character of the rock sequence of the Taknar Formation can be divided into lower, middle and upper members (Muller and Walter, 1983):

The lower member crops out in the central part of Taknar Inlier and is characterized by an alternation of uniform dark tuffs to dark-gray rhyolites with one light-gray rhyolite flow extends 120 m in thickness.

The middle member is exposed along the northern and southern margins of Precambrian uplift. It begins with the first

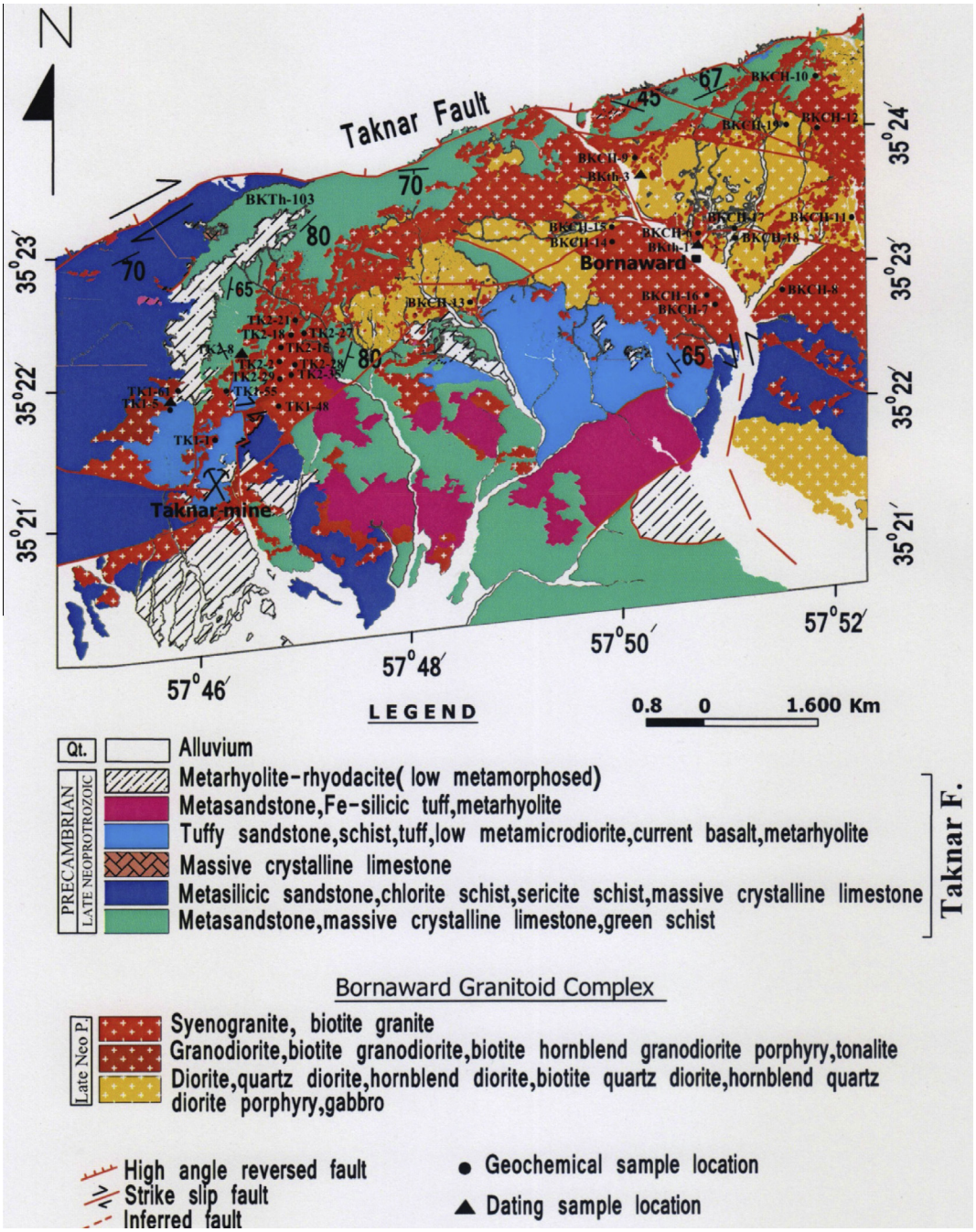

Fig. 2. Simplified geological map of the Bornaward region. Locations of dating and geochemical samples are shown.

alternation of carbonates and sandstones and has an estimated thickness of 150–350 m. According to the lithological and petrological characters of the volcanics of the lower and middle Taknar Formation, five rock types can be recognized as follows:

1 – Light rhyolites, 2 – dark-gray to nearly black rhyolites, 3 – green–gray rhyolites, 4 – gray to dark green uniform tuffs, 5 – light-green to green bounded tuffs.

In the western part of Taknar Inlier, a series of the green shales and sandstones form the base of an Infracambrian to Ordovician rock sequence. The sequence which is considered to be the upper part of Taknar Formation (Upper Taknar member) consists of a monotonous alternation of green and gray phyllitized shales and slates (Muller and Walter, 1983). The Taknar Inlier forms an uplift of the Central Iranian Precambrian–Paleozoic continental crust basement.

A complex of intrusive rocks exists in the Taknar zone that is named "Bornaward Granitoid Complex" (BGC) (Fig. 1). The intrusive rocks consist of granite, alkaligranite, syenogranite, leucogranite, granophyre, monzogranite, granodiorite, biotite granodiorite, biotite hornblende granodiorite, tonalite, diorite, quartz diorite, hornblende diorite, biotite quartz diorite, microdiorite, gabbro and microgabbro.

Granite, granodiorite and diorite are dominant (Fig. 2). Most development of the granite and granodiorite intrusions is exposed in the east, center and west of the study area, and also in the Taknar mine with more extension, as it cuts massive sulfide ore body and the Taknar Formation. Basic intrusions, particularly, diorite outcrops, are exposed in the middle of Bornaward Granitoid Complex.

Based on field observations and zircon U–Pb dating, it is proved that diorite and gabbro are older than acidic rocks. The acidic bodies surrounded the basic bodies which are located in the center of complex (Fig. 2). The Bornaward granitic rocks cut through the metamorphic rocks of the Taknar Formation. Since the Taknar Zone is an exotic block and it is surrounded by two major faults (Darouneh and Taknar). In some locations, along the faults were formed gneiss, mylonite and amphibolite rocks.

The Taknar mine is a magnetite-rich polymetal (Cu, Zn, Au, Ag, and Pb) massive sulfide deposit. Mineralization shows good layering, therefore, it is a syngenetic deposit formed at certain horizons within the upper member of Taknar Formation. Malekzadeh Shafaroudi (2004) and Ghoorchi (2004) worked on the geology, alteration and mineralization of Taknar deposit.

3. Petrography of Bornaward Granitoid Complex

The early magmatic episode in the Bornaward area is characterized by the occurrence of diorite. After this, tonalite and granodiorite intruded into basic rocks. Granite represents the late stage intrusive episode which occurs extensively in the Bornaward area. The petrography of Bornaward Granitoid Complex rocks is follows:

3.1. Bornaward Granitoid Complex

3.1.1. Diorite

These rocks have hypidiomorphic granular, allotriomorphic granular and slightly porphyritic textures. These rocks contains coarse grains including 35–39 vol.% plagioclase, 30–36 vol.% green hornblende, and 2–4 vol.% quartz in groundmass and also as phenocryst and anhedral with undulatory extinction. Plagioclases usually have normal zoning and are highly altered to sericite. Other alteration minerals include epidote, zoisite and clinozoisite. Accessory minerals contain zircon, apatite, magnetite, rutile, zircon and Fe–Ti oxides. Due to regional metamorphism and alteration, both plagioclase and hornblende have altered to chlorite and carbonate.

3.1.2. Monzogranite

These rocks have hypidiomorphic granular and are slightly porphyritic textures. The mineralogy of unit contains 18–25 vol.% fine to coarse anhedral quartz grains in the groundmass and also as a phenocryst it shows undulatory extinction, recrystallization, ridged margins and subgrains. All of these are reasons of the effects of tectonic deformation. Other minerals are plagioclase (28–35 vol.%) which generally shows effects of sericitization and formed as phenocryst and in background rock, and 30–38 vol.% K-feldspar (orthoclase and microcline) as phenocryst and in the groundmass forming pertitic texture. Also, biotite exists in low contents (4–7 vol.%) and is hardly chloritized.

3.1.3. Tonalite

The tonalite has granular and micro-pertitic textures. The mineralogy of rock contains 36–40 vol.% euhedral to subhedral plagioclase (oligoclase or andesine) minerals with a size up to 4 mm long and normal compositional zoning, 25–33 vol.% subhedral amphibole grains, 15–24 vol.% quartz, 5–7 vol.% biotite, and 4–6 vol.% K-feldspar. Accessory minerals include apatite, sphen, zircon and magnetite.

3.1.4. Granodiorite

The granodiorites have hypidiomorphic granular, micro-pertitic and sometimes microgranophyric, porphyritic and graphic intergrowth textures. These rocks contains 18–26 vol.% anhedral quartz grains with wavy extinction, recrystallization, ridged margins and subgrains. These are reasons of the effects of the dynamic metamorphism. Other minerals contain 16–24 vol.% K-feldspar (orthoclase and microcline with micro-pertitic texture) in the groundmass and as phenocryst, plagioclases usually have normal compositional zoning and an average of 45 vol.% (ranging from 36% to 58%) with polysynthetic and pericline twins, 10 vol.% green and brown fine grain biotite between quartz and plagioclase grains, 4–9 vol.% green hornblende. Accessory minerals include sphene, zircon, and apatite annexed in biotite, ilmenite and magnetite.

3.1.5. Granite

Field observations show that granites are the latest intrusive episode in the Bornaward Granitoid Complex. The contact of granite with surrounded rocks (tonalite, granodiorite and diorite) is sharp. At external contacts, the granite intrudes into very low-grade metavolcanic rocks of the Taknar Zone.

Majority of the rocks have micrographic, micro-pertite, granophyric, idiomorphic granular, hypidiomorphic granular, granular and slightly porphyritic textures. These rocks have composed of 33–35 vol.% fine to coarse-grained quartz in the groundmass and also appendixed in alkali-feldspar. Majority of quartz grains are anhedral, undulatory extinction, recrystallization, ridged margins and subgrains. These are reasons of the effects of tectonic deformation. In these rocks, plagioclase shows strong resorption along margins and only small anhedral plagioclase grains occur in some samples. Other minerals contain 24–29 vol.% K-feldspar (orthoclase and microcline) as phenocryst and also in the groundmass form granophyric texture, 20–27 vol.% plagioclase with polysynthetic and pericline twins and oscillatory zoning, and 8 vol.% green and brown fine grain biotite. Accessory minerals include magnetite, ilmenite, zircon, sphene, epidote, zoisite and clinozoisite.

3.1.6. Spotted granite

Small outcrops of spotted granite crops out only in the Taknar mine. They have porphyritic texture with elongated black ellipsoids. These elongated ellipsoids formed during regional

metamorphism and along the fault movements. The ellipsoids consist of chlorite, quartz & opaque minerals.

3.1.7. Alkali granite

This rock is a medium-grain-size rock 3–5 mm with a light cream to pinkish color. The rock lack amphibole and includes 48–57 vol.% micro-pertite, 30–39 vol.% quartz and 4–7 vol.% sparse crystals of biotite. The presence of abundant microcline suggests balance at a very low temperature in the plutonic environment (Gribble, 1988). Other accessory minerals include ilmenite, zircon, and titanite.

3.1.8. Leucogranite

These acidic rocks, in general, are medium to coarse grained, with granular, hipidiomorphic granular and micro-pertitic textures. The mineral composition composed of 37–45 vol.% K-feldspar as subhedral and anhedral microcline or orthoclase with micro-pertitic texture. Plagioclase minerals generally show kinking and breaking as a result of stress and tectonic deformation. Also, the rocks have 45–55 vol.% ubiquitous quartz that usually occur in single grains or in irregular aggregates with an highly variable size. 8–10 vol.% tabular plagioclase is subhedral and euhedral and shows exsolution of microcline patches. Its composition is albite to oligoclase with reverse zonation. Also, 2–3 vol.% green and brown biotite is subhedral to anhedral. Zircon crystals exhibit prismatic to round shape with oscillatory zoning. Majority of quartz grains are anhedral and show undulatory extinction, recrystallization, ridged margins and subgrains. These are reasons for the effect of tectonic deformation and highly dynamic metamorphism in the rocks. Accessory minerals are sphene, zircon, ilmenite, epidote, zoisite and clinozoisite and opaque minerals. Alteration minerals include kaolinite and sericite.

3.1.9. Granophyre

The Bornaward granophyre rocks have allotriomorphic granular, micrographic, granophyric and porphyritic textures. The rocks are composed of 35–46 vol.% fine and coarse anhedral quartz grains in the groundmass and into alkali-feldspar grains as micrographic texture, 48–57 vol.% K-feldspar (orthoclase and microcline) as phenocryst and also in the groundmass that form micrographic texture as a characteristic of the granophyre rocks, 18–24 vol.% plagioclase, and 3–5 vol.% green and brown fine grain biotite. Accessory minerals include magnetite, zircon, apatite and ilmenite.

3.2. Microgranular enclaves

The BGC rocks have microgranular enclaves with compositions of semi- to similar of host rocks. The enclaves which exist in the granites have granitic composition and low alteration. Also, their rims have chilled margins. The shape and size of enclaves are very different and their shapes are irregular. The enclaves which exist in the granodiorites are rich from biotite, plagioclase and quartz. The composition of enclaves of the BGC rocks are tonalitic to granodioritic. These enclaves are more regular than granitic types and it seems that they have transported from deeper levels.

Generally, it seems that the enclaves which exist in the leucogranites are related to shallow levels and last emplacement stages. The enclaves related to deep levels are rare or absent.

4. Analytical techniques

4.1. Bulk-rock chemistry

Representative samples of the Bornaward Granitoid Complex rocks were analyzed for rare earth and trace elements by using ICP-MS at the Acme Lab (Canada). Major oxides containing SiO_2, Al_2O_3, Na_2O, MgO, K_2O, TiO_2, MnO, CaO, P_2O_5, Fe_2O_3 and L.O.I were measured by X-ray fluorescence spectrometry (XRF) method in the Analytical Geology Lab. of Spectrum Kansaran Binaloud in Iran. Trace elements including Ba, Be, Co, Cs, Ga, Hf, Nb, Rb, Sn, Sr, Ta, Th, U, V, W, Zr, Y and REE were determined by Inductively Coupled Plasma-Mass Spectrometer (ICP-MS) in Acme Analytical Laboratories (Vancouver, Canada). Detection limit of trace elements and REE in the research is between 0.01 and 8 ppm.

4.2. Zircon U–Pb dating

The analyzed zircons in the study were separated by using the standard heavy liquid (Bromoform) and magnetic procedures, from 5 kg samples of collected from the BGC outcrops. From each rock were separated about 50 zircon grains. The Zircons were mounted along with a zircon standard and a couple of NBS 610 Trace Element Glass chips in epoxy and then were polished down to 20 μm. The zircons age dating were done at the Arizona Laser Chron Center. The U–Pb isotope data were collected by using a New Wave 193 nm ArF laser ablation system coupled to a Nu Plasma HR Inductively Coupled Plasma-Mass Spectrometer (ICP-MS) at the Arizona Laserchron Center according to methods of described by Gehrels et al. (2008). Concordia diagrams were obtained by using the ISOPLOT software (Ludwig, 2003).

All of the zircons were examined by using a combination of Cathodoluminescence (CL) and optical microscopy prior to analysis. Cathodoluminescence images are acquired for samples to be analyzed because they provide a powerful tool for placing laser pits in homogeneous portions of crystals. They can also help to determine the origin (e.g., igneous, metamorphic, hydrothermal) of zircon grains. Laser ablation takes place with a beam diameter of either 35 or 25 μm for most applications, or with a beam diameter of 15 or 10 μm if finer spatial resolution is needed. With a 35 or 25 μm beam, the laser is set at a repetition rate of 8 Hz and energy of 100 mJ, which excavates at a rate of ~1 μm per second. This generates a signal of ~100,000 cps per ppm for U in zircon. Isotopic analysis is performed with a Multicollector Inductively Coupled Plasma mass spectrometer (GVI Isoprobe) that is equipped with an S-option interface. The instrument is equipped with a collision cell that is operated with a flow rate of 0.2 ml/min of Argon and the accelerating voltage is ~6 kV to create a uniform energy distribution.

5. Zircon morphology and Th/U ratios

In all of the U–Pb dated Bornaward Granitoid Complex rocks samples, the zircon grains are colorless and/or yellow to pale yellow, transparent and commonly euhedral. The range of size of zircon grains is 70–420 μm; the grains have a length/width ratio of 1:1–6:1. Based on cathodoluminescence images, the majority of zircons in the four analyzed samples, including two samples of granites (BKTh-1, TAK2-8), granodiorite (TAK1-5) and diorite (BKTh-3), are coarse grain and have a zoning shape, but some of them have a prismatic form. Most of the zircons in the granite samples are medium elongated, low rounded and distinctly crystalline. The length of zircons in the granite samples are 100–230 μm and their width is 70–120 μm (Fig. 3A). Also, the size of zircons of the diorite are more than the granites, however the range of length and width of zircons in the diorite is 200–420 μm and 100–200 μm, respectively (Fig. 3B).

In general, when shape and morphology are problematic for classifying zircons, their compositions yield information about their origin. Additionally, the Th/U ratio can be used to determine the origin of zircon. The Th/U ratio is usually higher in magmatic

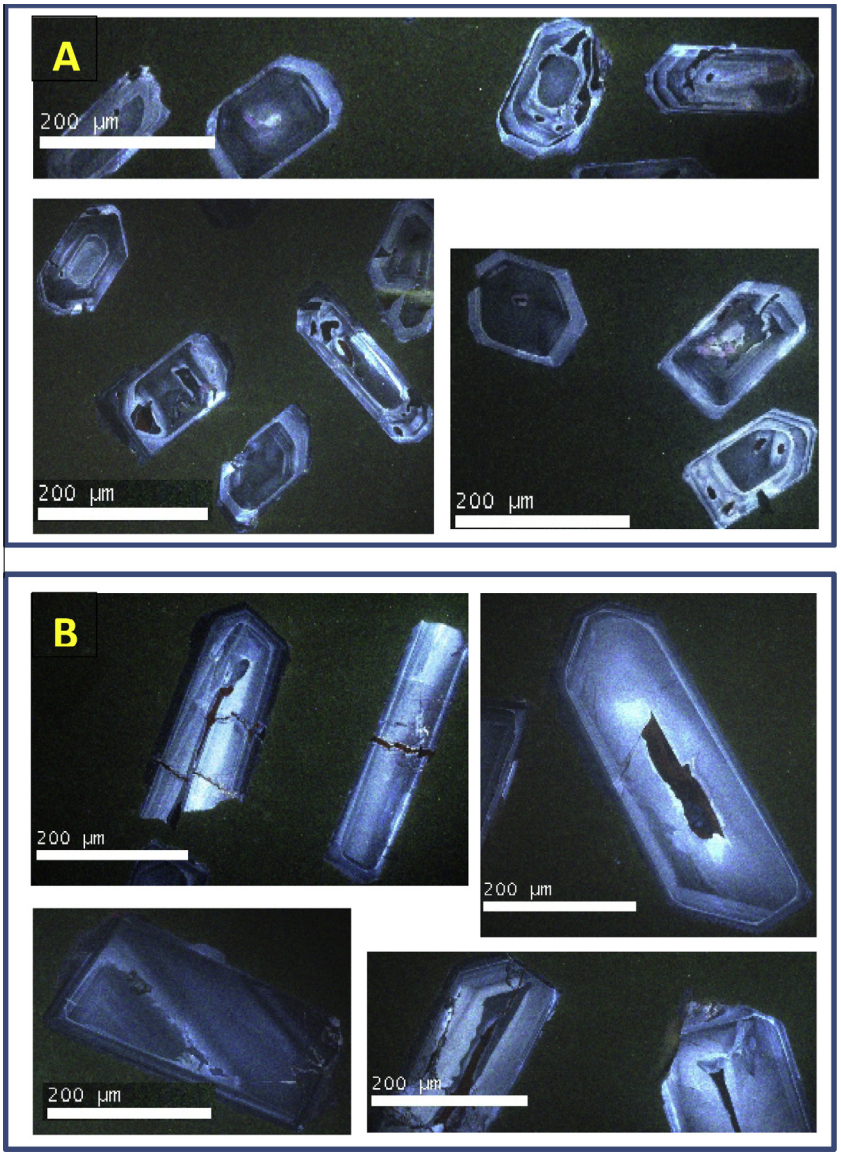

Fig. 3. Cathodoluminescence images of zircon belong to granite (A) and diorite (B).

zircon than in metamorphic zircon. For example, low ratios of <0.31 indicate a metamorphic origin, and very low ratios, in the range of 0.02–0.11, indicate a metamorphic origin (Chen et al., 2007). Fuping et al. (2007) showed that zircons with high Th/U ratios (0.15–1.37) imply magmatic events, and zircons with low Th/U ratios (0.06–0.34) indicate metamorphic origin. The chemical composition of the zircons in the granite (BKTh-1) and the diorite (BKTh-3) imply that most of the zircons have high Th/U ratios and they have magmatic origin. The majority of Th/U ratios in the granites at the study are 0.41–1.20 and in the diorite are 0.14–1.25.

6. Sr–Nd isotopes

The Sr and Nd isotopic analyses of four whole rock samples were performed on a 6-collector Finnigan MAT 261 Thermal Ionization Mass Spectrometer at the University of Colorado, Boulder (USA). The $^{87}Sr/^{86}Sr$ ratios were analyzed by using four-collector static mode measurements. Thirty measurements during the study yielded mean $^{87}Sr/^{86}Sr = 0.71032 \pm 2$ (error is the 2σ mean). The measured $^{87}Sr/^{86}Sr$ were corrected to SRM-987 = 0.71028. Error in the 2σ of mean refers to the last two digits of the $^{87}Sr/^{86}Sr$ ratio. The measured $^{143}Nd/^{144}Nd$ were also normalized to $^{146}Nd/^{144}Nd = 0.7219$. The analyses were dynamic mode, three-collector measurements. Thirty-three measurements of the La Jolla Nd standard during the study period yielded a mean $^{143}Nd/^{144}Nd = 0.511838 \pm 8$ (error is the 2 sigma mean).

7. Geochemistry

7.1. Major and trace element characteristics

Representative rocks of the BGC were analyzed for major, trace elements and rare earth elements (Table 1). The rocks of Bornaward Granitoid Complex have a wide range of chemical compositions, with $SiO_2 = 65.03–77.02\%$, $Al_2O_3 = 10.93–13.66\%$, $MgO = 0.01–2.27\%$, $FeO = 1.01–10.35\%$ (based on total Fe), $CaO = 0.21–4.37\%$, (Major oxides data Repository, Table 1). They are relatively high in total alkalis, with $K_2O = 0.55–5.83\%$, $Na_2O = 0.28–7.02\%$, the sum of the $K_2O + Na_2O$ ranging from 4.76% to 8.70%, and low abundances of MnO, P_2O_5 and TiO_2 (Table 1). The chemical composition of 27 samples of the BGC were

Table 1
Chemical compositions of representative rock samples from the Bornaward and Taknar areas.

Sample no.	BKCH-6	BKCH-7	BKCH-8	BKCH-9	BKCH-10	BKCH-11	BKCH-12	BKCH-13	BKCH-14	BKCH-15
Sample	57°50′48″	57°50′57″	57°51′29″	57°50′09″	57°51′50″	57°52′09″	57°51′55″	57°48′34″	57°49′54″	57°49′43″
Location	35°23′11″	35°22′37″	35°22′44″	35°23′42″	35°24′25″	35°23′17″	35°23′58″	35°22′39″	35°23′11″	35°23′13″
Rock type	High Fe_3O_4-granite	Granite	Granophyre	High Fe_3O_4-tonalite	Leucogranite	Granite	Granophyre	Granite	Granite	Monzogranite
SiO_2	67.94	75.44	76.53	65.03	75.85	75.51	75.65	75.71	74.98	67.84
TiO_2	0.95	0.26	0.26	0.72	0.23	0.23	0.24	0.29	0.23	0.73
Al_2O_3	11.73	12.73	11.39	11.09	12.68	12.17	12.31	11.98	12.92	12.47
FeOt	8.5	1.83	2.52	10.35	2.07	2.17	2.58	4.12	2.07	7.19
MnO	0.08	0.02	0.02	0.23	0.02	0.03	0.02	0.04	0.02	0.09
MgO	1.14	0.15	0.24	2.27	0.14	0.21	0.08	0.07	0.01	2.18
CaO	2.73	0.55	0.43	4.37	0.21	0.88	0.41	0.57	0.32	3.11
Na_2O	3.55	4.02	3.62	3.93	5.19	3.77	4.22	3	3.67	2.52
K_2O	2.71	3.66	3.84	1.1	2.3	3.72	3.07	3.45	4.02	2.86
P_2O_5	0.18	0.04	0.04	0.21	0.03	0.03	0.03	0.04	0.04	0.2
L.O.I	0.79	0.91	0.74	1.69	0.8	0.68	0.82	1.58	1.16	1.38
Total	100.3	99.61	99.63	100.99	99.52	99.4	99.43	97.69	99.44	100.57
Ba	582	556	663	302	390	716	533	672	745	732
Co	53	1	4	73	5	8	16	16	2	33
Cs	2.6	0.5	0.3	0.4	0.2	0.3	0.5	1.3	0.4	4.6
Ga	19.6	15.5	15.9	12.7	15.9	16.5	14.9	16.7	15.4	17.8
Hf	23.8	7.5	7	1.6	7.3	7.7	7.3	8.1	7.6	6.7
Nb	22.7	10.9	10.6	1.2	10.6	12.3	11.4	12.1	12.4	9.8
Rb	85	55.8	51.5	13.8	28	76.2	56.9	60.6	94.4	100
Sr	122.2	49.5	30.4	253.9	56.4	61.6	37.4	51.1	31.6	229
Ta	1.6	1	0.9	<0.1	1	1	1	0.9	1.1	0.7
Th	23	26	24	2	27	24	18	19	29	11
V	144	52	49	122	47	49	49	52	51	101
Zr	916.7	245.8	239.3	50.8	258.2	250.7	239.5	287.4	260.6	269.1
Y	208	75	67	33	73	114	96	79	88	44
La	40.5	36.6	31.6	5.1	38.6	55.5	42.1	38	40.7	39.2
Ce	88.2	78.5	66	12.1	78.1	119.3	89.6	80.1	81.4	75.1
Pr	11.19	9.13	7.69	1.75	8.68	13.16	10.15	8.74	9.02	8.38
Nd	47.5	38.1	28.4	7.8	34.3	53.3	40.5	34	35.4	31.4
Sm	12.23	8.5	6.99	2.63	7.71	10.99	9.18	7.74	7.67	6.22
Eu	2.47	1.13	0.69	0.89	1.11	1.23	1.3	1.09	1.21	1.46
Gd	12.07	7.77	6.62	3.05	7.44	10.2	8.81	7.6	7.24	5.46
Tb	2.49	1.52	1.31	0.64	1.44	1.9	1.65	1.45	1.38	0.92
Dy	14.3	8.43	7.61	3.57	8.77	10.53	10.17	8.41	7.82	4.81
Ho	3.43	1.81	1.8	0.92	1.93	2.37	2.12	1.87	1.79	1.11
Er	10.09	5.48	5.1	2.89	6.28	6.47	6.33	5.51	5.15	2.98
Tm	1.52	0.79	0.73	0.41	0.88	0.98	0.91	0.8	0.79	0.42
Yb	9.64	5.32	4.97	2.64	6.15	6.56	5.54	5.19	5.08	2.97
Lu	1.55	0.84	0.73	0.44	0.9	1.01	0.88	0.83	0.81	0.42
REE	257.2	203.2	170.2	44.8	202.3	293.5	229.2	201.33	205.5	180.9
$(La/Yb)_N$	2.27	3.72	3.43	1.04	3.39	4.57	4.11	3.96	4.33	7.13
CaO/Na_2O	0.77	0.14	0.12	1.11	0.04	0.23	0.1	0.19	0.09	1.23
Al_2O_3/TiO_2	12.35	48.96	43.81	15.4	55.13	52.91	51.29	41.31	56.17	17.08
$Na_2O + K_2O$	6.26	7.68	7.46	5.03	7.49	7.49	7.29	6.45	7.69	5.38
Rb/Sr	0.69	1.13	1.69	0.05	0.49	1.24	1.52	1.18	2.99	0.43
Rb/Ba	0.15	0.1	0.08	0.04	0.07	0.1	0.1	0.1	0.13	0.14
Th/Yb	2.38	4.89	4.83	0.76	4.39	3.66	3.25	3.66	5.71	3.7
Ta/Yb	0.16	0.19	0.18	0.04	0.16	0.15	0.18	0.17	0.21	0.23

Sample no.	BKCH-16	BKCH-17	BKCH-18	BKCH-19	TK2-18	TK1-61	TK2-15	TK2-28	TK1-5
Sample	57°50′46″	57°51′00″	57°50′56″	57°51′31″	57°46′50″	57°45′43″	57°46′42″	57°46′53″	57°45′57″
Location	35°22′40″	35°23′14″	35°23′13″	35°24′01″	35°22′24″	35°22′01″	35°22′18″	35°22′15″	35°21′58″
Rock type	Granodiorite	Granodiorite	Granodiorite	Granodiorite	Granite	Granodiorite	Granite	Granite	Granodiorite
SiO_2	73.04	75.41	75.58	77.02	76	68.53	71.48	71.75	72.68
TiO_2	0.41	0.24	0.25	0.22	0.1	0.75	0.19	0.22	0.26
Al_2O_3	12.76	12.12	12.09	11.48	10.93	12.01	12.61	13.63	12.73
Fe_2O_3					1.6	2.25	1.69	1.72	1.76
FeOt	3.21	1.85	2.3	1.22	1.08	3.28	3.09	1.01	1.49
MnO	0.04	0.03	0.03	0.03	0.01	0.1	0.04	0.03	0.05
MgO	0.4	0.23	0.1	0.25	0.06	1.44	0.34	0.2	1.63
CaO	0.98	0.9	0.69	1.38	0.89	1.13	0.36	0.7	0.8
Na_2O	3.4	4.02	3.3	4.06	0.28	2.99	2.04	7.02	2.76
K_2O	4.11	3.63	4.39	3.32	5.83	2.34	4.99	1.06	3.04
P_2O_5	0.06	0.03	0.03	0.03	0.06	0.2	0.08	0.08	0.06
L.O.I	0.81	0.95	0.66	0.64	1.91	3.02	1.57	0.53	1.6
Total	99.22	99.41	99.42	99.65	98.75	98.04	98.48	97.95	98.86
Ba	1037	640	815	656	1656	573	1974	205	622
Co	16	14	11	N	3.4	7.3	3.4	4.1	2.4
Cs	1.1	0.8	0.5	0.1	1.8	3.3	1.6	0.7	1.7

Table 1 (*continued*)

Sample no.	BKCH-16	BKCH-17	BKCH-18	BKCH-19	TK2-18	TK1-61	TK2-15	TK2-28	TK1-5
Sample	57°50′46″	57°51′00″	57°50′56″	57°51′31″	57°46′50″	57°45′43″	57°46′42″	57°46′53″	57°45′57″
Location	35°22′40″	35°23′14″	35°23′13″	35°24′01″	35°22′24″	35°22′01″	35°22′18″	35°22′15″	35°21′58″
Rock type	Granodiorite	Granodiorite	Granodiorite	Granodiorite	Granite	Granodiorite	Granite	Granite	Granodiorite
Ga	16.5	16.1	16.1	14.5	12.5	15.4	16.4	17.6	16.3
Hf	9.5	6.9	8.3	7.9	4.4	12.8	5.6	6.5	7.4
Nb	11.1	12.8	11.9	11	8.9	13	10.5	10.3	12.6
Rb	74.8	57.8	92.6	33.2	107	97.9	124.3	31.9	142.1
Sr	81.6	59.5	50	72.7	36.8	138.3	53.6	101.3	40
Ta	0.8	1.1	0.9	0.8	0.7	1	0.9	0.7	1.1
Th	22	19	19	27	14.8	16.2	18	20.8	214.4
V	68	49	49	43	<8	75	<8	<8	11
Zr	333.1	245.2	279.2	242.6	116.2	437.2	167.8	200.6	21.8
Y	66	86	77	86	60	27.7	32	43.3	72.9
La	36.3	39.1	36	48.9	42.1	43.7	12.6	45.2	36.1
Ce	77.2	81.1	77.5	103.6	82.6	94.6	44.6	92.5	79.2
Pr	8.74	9.57	9.61	11.31	8.7	10.4	4.01	10.6	9.48
Nd	36.2	39.2	39	44.7	3.3	38.8	16.2	41	35.2
Sm	7.86	9.27	9.36	9.18	7.18	7.01	3.41	7.93	8.24
Eu	1.39	1.18	1.12	1.16	0.64	1.37	0.33	1.24	0.92
Gd	7.29	9.29	9.31	8.66	7.59	5.7	3.21	7.3	8.89
Tb	1.36	1.76	1.74	1.62	1.58	0.93	0.66	1.27	1.81
Dy	7.84	9.62	9.87	9.51	10.04	5.13	4.45	7.49	11.71
Ho	1.73	2.07	2.07	2.05	2.05	1	1.05	1.56	2.45
Er	5.18	6.27	5.9	6.09	6.13	2.92	3.66	4.51	7.37
Tm	0.71	0.86	0.79	0.86	0.78	0.37	0.5	0.6	0.94
Yb	4.63	5.64	5.84	6.35	5.45	2.99	3.96	4.67	6.98
Lu	0.74	0.85	0.86	0.91	0.77	0.45	0.62	0.7	0.96
REE	197.2	215.8	209	254.9	208.91	215.37	99.26	226.36	210.25
$(La/Yb)_N$	4.24	3.75	3.33	4.16	4.17	7.9	1.72	5.23	2.79
CaO/Na_2O	0.29	0.22	0.21	0.34	3.56	0.38	0.17	0.1	0.29
Al_2O_3/TiO_2	31.12	50.5	48.36	52.18	109.3	16.01	66.37	61.95	48.96
$Na_2O + K_2O$	7.51	7.65	7.69	7.38	6.11	5.33	7.03	8.08	5.8
Rb/Sr	0.92	0.97	1.85	0.45	2.9	0.7	2.32	0.31	3.55
Rb/Ba	0.07	0.09	0.11	0.05	0.06	0.17	0.06	0.15	0.23
Th/Yb	4.75	3.37	3.25	4.25	2.71	5.42	4.54	4.45	3.12
Ta/Yb	0.17	0.19	0.15	0.12	0.13	0.33	0.23	0.15	0.16
Sample no.	TK2–2	TK2-35	TK2-27	TK1-48	TK2-29	TK1-1	TK1-55	TK2-21	TK1-5
Sample	57°46′38″	57°46′47″	57°46′58″	57°46′22″	57°46′36″	57°46′13″	57°46′18″	57°46′54″	57°45′57″
Location	35°22′15″	35°22′10″	35°22′26″	35°21′53″	35°22′09″	35°21′39″	35°22′06″	35°22′32″	35°21′58″
Rock type	Granite	Granodiorite	Granite	Granite	Granodiorite	Granite	Granite	Granite	Granodiorite
SiO_2	75.05	71.55	71.98	69.77	71.61	68.93	69.87	70.8	72.68
TiO_2	0.13	0.17	0.2	0.17	0.16	0.42	0.14	0.16	0.26
Al_2O_3	11.48	13.66	12.43	13.29	12.06	12.58	12.25	13	12.73
Fe_2O_3	1.63	1.67	1.7	1.67	1.66	1.92	1.64	1.66	1.76
FeO	1.85	2.49	1.6	2.73	2.12	3.3	3.66	2.6	1.49
MnO	0.04	0.04	0.03	0.06	0.03	0.06	0.01	0.02	0.05
MgO	n.d	0.62	0.35	1.52	1.32	0.56	0.28	0.42	1.63
CaO	0.61	0.87	0.52	0.41	1.02	0.67	0.44	0.48	0.8
Na_2O	6.15	1.4	4.66	2.69	2.66	3.63	4.44	4.69	2.76
K_2O	0.55	3.36	4.04	4.45	3.71	4.01	3.28	3.49	3.04
P_2O_5	0.03	0.06	0.08	0.08	0.04	0.1	0.04	0.07	0.06
L.O.I	1.2	2.33	0.41	1.48	0.99	1.22	1.07	1.27	1.6
Total	98.72	98.22	98	98.32	97.38	97.4	97.12	98.66	98.86
Ba	330	1311	1854	1755	1299	2779	629	981	622
Co	3	3.7	1.3	2.5	2.2	3.4	13	2.8	2.4
Cs	0.5	0.8	0.9	1.9	2.6	2.7	1.4	0.8	1.7
Ga	15.3	17	18.3	16.8	16.2	16.2	14.2	16.3	16.3
Hf	6.1	5.9	5.9	6.2	5.1	7.5	4.7	6	7.4
Nb	11.2	10.8	12	10.6	10.6	11	10.8	11.4	12.6
Rb	34.5	91.7	63.8	134.2	127.3	117.3	78.3	130.4	142.1
Sr	72	66.9	89.2	55.1	110.9	112.9	102.4	65.1	40
Ta	0.9	1	0.9	0.8	0.9	0.9	1	0.9	1.1
Th	18	18.3	176.6	17.8	19.3	19.7	20.2	168.9	214.4
V	<8	<8	<8	<8	<8	32	10	<8	11
Zr	169.8	164.2	21	170.9	137.7	241.8	122.9	19	21.8
Y	49.6	65.6	48.3	52.3	50.5	47.7	38.9	54.3	72.9
La	42.5	44.7	45	32.6	34.3	31.6	38.4	31.4	36.1
Ce	90.8	99.1	97.5	79.8	77.9	71.7	81.7	71.5	79.2
Pr	10.8	12	11.4	8.67	9.21	8.66	9.95	8.48	9.48
Nd	42.1	45.3	43.9	34	34	34.9	37.1	33.1	35.2
Sm	8.56	10.05	8.63	7.03	7.54	6.95	7.6	7.08	8.24
Eu	1.01	0.97	1.12	0.76	0.56	0.82	0.82	0.59	0.92
Gd	8.35	10.15	7.87	7.17	7.4	6.77	6.61	6.92	8.89

(*continued on next page*)

Table 1 (*continued*)

Sample no.	TK2–2	TK2-35	TK2-27	TK1-48	TK2-29	TK1-1	TK1-55	TK2-21	TK1-5
Sample	57°46′38″	57°46′47″	57°46′58″	57°46′22″	57°46′36″	57°46′13″	57°46′18″	57°46′54″	57°45′57″
Location	35°22′15″	35°22′10″	35°22′26″	35°21′53″	35°22′09″	35°21′39″	35°22′06″	35°22′32″	35°21′58″
Rock type	Granite	Granodiorite	Granite	Granite	Granodiorite	Granite	Granite	Granite	Granodiorite
Tb	1.53	1.88	1.4	1.38	1.42	1.26	1.14	1.38	1.81
Dy	8.82	11.18	8.26	8.32	8.66	7.55	6.85	8.81	11.71
Ho	1.84	2.2	1.7	1.79	1.77	1.62	1.34	1.87	2.45
Er	5.43	6.42	5	5.38	5.18	4.93	3.77	5.65	7.37
Tm	0.71	0.85	0.65	0.7	0.68	0.65	0.53	0.73	0.94
Yb	5.46	6.16	4.9	5.03	5.23	5.14	4	5.48	6.98
Lu	0.78	0.85	0.72	0.75	0.74	0.75	0.59	0.8	0.96
REE	228.68	251.81	238.05	193.38	194.59	183.3	200.4	183.79	210.25
$(La/Yb)_N$	4.21	3.92	4.96	3.5	3.54	3.32	5.19	3.1	2.79
CaO/Na_2O	0.1	0.62	0.11	0.15	0.38	0.18	0.1	0.1	0.29
Al_2O_3/TiO_2	88.3	80.35	62.15	78.17	75.37	29.95	87.5	81.25	48.96
$Na_2O + K_2O$	6.7	4.76	8.7	7.14	6.37	7.64	7.72	8.18	5.8
Rb/Sr	0.48	1.37	0.71	2.43	1.15	1.04	0.76	2	3.55
Rb/Ba	0.1	0.07	0.03	0.07	0.1	0.04	0.12	0.13	0.23
Th/Yb	3.29	2.97	4.28	3.54	3.69	4.76	5.05	3.47	3.12
Ta/Yb	0.16	0.16	0.18	0.16	0.17	0.17	0.25	0.16	0.16

plotted in TAS diagram (Middlemost Eric, 1994) and they fall into the fields of granite, granodiorite and tonalite (Fig. 4). Maniar and Piccoli (1989) divided granitoids to three groups by using A/CNK-A/NK plot: (1) peraluminous, (2) metaluminous and (3) peralkaline. Most of the BGC rocks are located in high metaluminous to middle peraluminous groups and their alumina-saturation index (ASI: molar $Al_2O_3/CaO + Na_2O + K_2O$) is 0.70–1.82 (Chappell and White, 2001) (Fig. 5). Moderately peraluminous granitoids contain biotite. They could be evolved from S-type granitoids. Most of the Bornaward intrusive rocks contain K_2O from >3 to 5.83 wt.%, and the K_2O/Na_2O ratio is between 0.82 and 1.39 (Table 1). Therefore, based on the SiO_2–K_2O diagram (Peccerillo and Taylor, 1976), most of these rocks belong to high-K (potassic) calc-alkaline series and some others belong to Calc alkaline series (Fig. 6). Mineral assemblages of the intrusive rocks (biotite, hornblende, and ilmenite) support an interpretation that they belong to the ilmenite-series of the oxidized granitoids (S-type granitoids). Accordingly, the Bornaward intrusive rocks which are consistent to their high metaluminous to middle peraluminous and high-K (potassic) calc-alkaline and some also calc-alkaline have the relatively low CaO content, moderate LREE contents, high Rb and high Rb/Sr ratios with the mean value of 1.31. These support the idea that these rocks are S-type granitoids (Chappell, 1999). However, some S-type samples have metaluminous affinity and display similarities with I-type granites in terms of high Na_2O, Sr and low Ce and Y content. This is also supported by some transitional compositions between the I- and S-type granitoids, caused by the more felsic, potassic and slightly peraluminous characters of some I-type granitoids, the absence of hornblende in some members and the negative correlation between P_2O_5 and SiO_2 due to the fractionation of apatite in the absence of Y-bearing accessory minerals (Chappell and White, 1992).

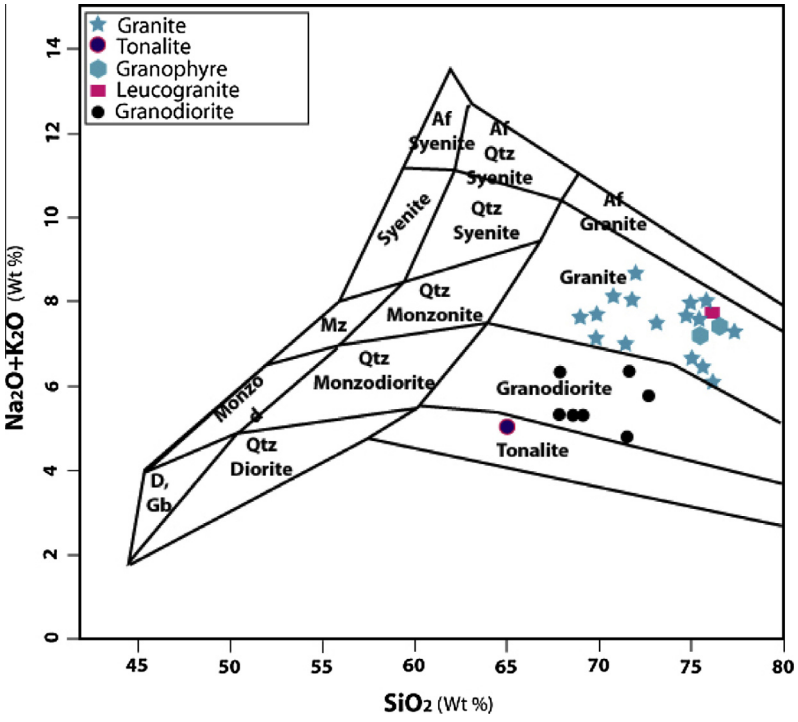

Fig. 4. Composition of the Bornaward granitoid plotted on the TAS diagram (Middlemost Eric, 1994).

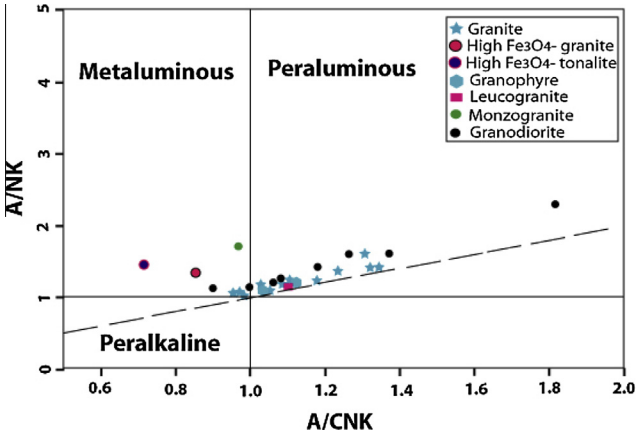

Fig. 5. Shand's molar parameters A/NK = $Al_2O_3/(Na_2O + K_2O)$ vs. A/CNK = $Al_2O_3/(CaO + Na_2O + K_2O)$ – Chappell and White (2001).

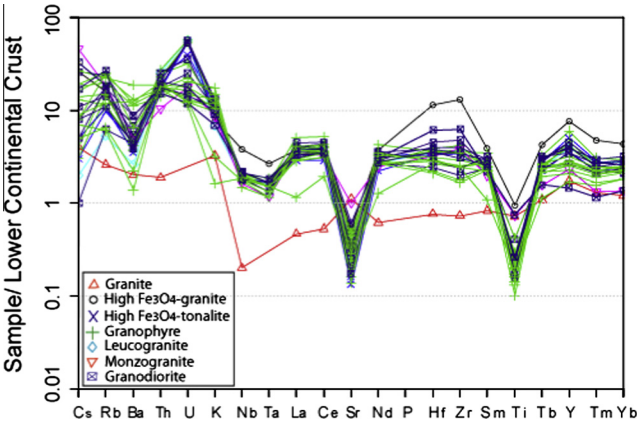

Fig. 7. Spider diagram for the Bornaward intrusive bodies. Data for Lower continental crust are from Taylor and McLennan (1995).

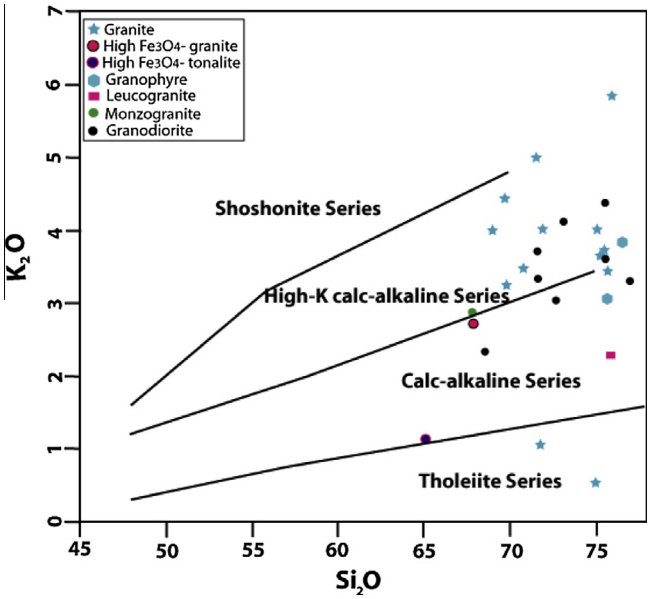

Fig. 6. K_2O vs. SiO_2 variation diagram with boundaries by for high-K, medium-K, and low-K magma series (Peccerillo and Taylor, 1976).

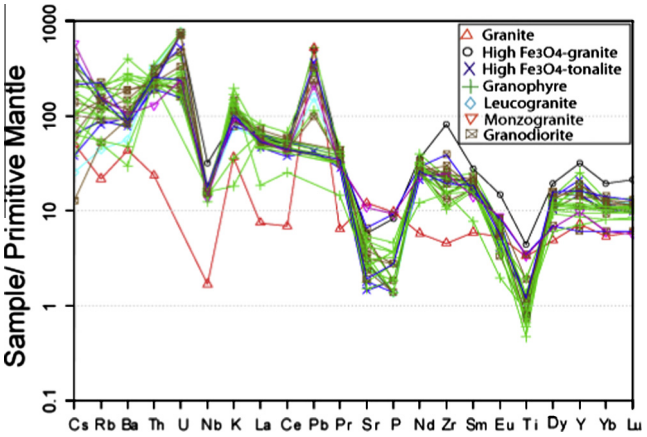

Fig. 8. Primitive-mantle-normalized trace element patterns for the intrusive rocks of the Bornaward region. Normalizing values are from Sun and McDonough (1989).

LILEs in the Bornaward intrusive rocks are relatively enriched (LILEs: Cs, Rb, Ba, K, La, Nd, Hf, Zr and Y) and other incompatible elements behave very similarly to LILE (Th and U), and also strongly depleted in high field strength elements (HFSE: Nb, Ta, Sr and Ti). In contrast to the LILEs, silica-rich rocks are relatively enriched in HFSE such as Nb, Y, V and Co (Table 1). The BGC rocks show very strong depletion in Sr and Ti, and high enrichment in U and slight enrichment Y, Hf and Zr (Fig. 7).

According to the data related to the rocks belong to the BGC, major and trace elements (Table 1), in the primitive-mantle-normalized trace element spider diagram (Sun and McDonough, 1989), Sr, Ba and Ti are roughly compatible and their concentrations decrease sharply in a linear array during the evolution of magma (Fig. 8). The Sr/Ba ratios only slightly decrease, whereas the Rb/Sr ratios exhibit a strong increase from low- to high-silica members in each granitoid suite. Based on the primitive mantle-normalized element pattern, the Bornaward Granitoid Complex is distinguished by the enrichment of large ion lithophile elements (LILEs: K, Cs, Rb, Ba) and the low HFSE contents (V, Cr, Co, Ni, Cu). Also, the negative Nb anomaly is very significant, specially the granites. Negative Sr and Eu anomalies can be explained by plagioclase fractionation.

Chemical composition of the Bornaward intrusive rocks are plotted in 10,000 × Ga/Al vs. trace element (Nb) and major oxides ($Na_2O + K_2O$) discrimination diagrams. They plot in the field of S & I-type granites (Whalen et al., 1987) (Fig. 9). A few of the Bornaward intrusive rocks have significantly higher HFSE and HREEs contents and ($K_2O + Na_2O$)/CaO ratios and also include magnetite, for example: magnetite-bearing granite and tonalite. They have high FeO_t, TiO_2, MgO and P_2O_5 contents and low SiO_2 content. Moreover, reduction Ti and P_2O_5 reveals that the separation of Fe–Ti oxides (ilmenite, titanomagnetite, and sphene), zircon and apatite controlled the variation of these elements. In general, the Bornaward biotites have low TiO_2 (<2.5 wt.%) (Soltani, 2000). The Ti content of biotite is mainly controlled by temperature and liquid composition. It appears to be particularly insensitive to fO_2 (Wyborn, 1983). Also, low TiO_2 content in biotite indicates possibly Ti depletion occurred at the source (e.g., Harrison, 1990).

7.2. Rare earth element (REE) patterns

In the granitic rocks, about 80–95% of the REE are held in sphene and allanite (Gromet and Silver, 1987). The separation of zircon was significant in the Bornaward granitoids. The REE data and the chondrite-normalized plot (McDonough and Sun, 1995) of representative samples of the BGC rocks are presented in

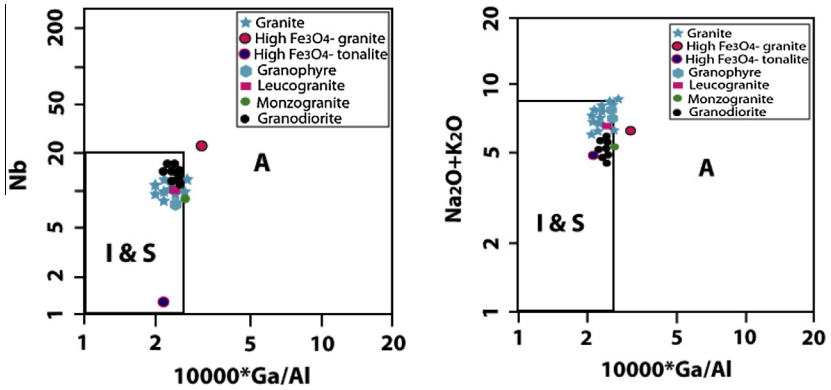

Fig. 9. The Bornaward granitoid rocks are plotted in the field of I, S and A type (Whalen et al., 1987).

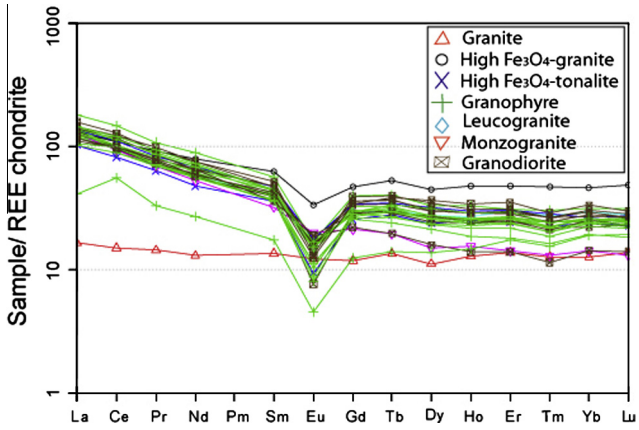

Fig. 10. Chondrite-normalized REE plot for selected whole-rock granitoid samples from the Bornaward region (Boynton, 1984).

Table 1 and in Fig. 10. The chondrite-normalized rare earth element (REE) plot indicate minor enrichments of heavy REE with $(La/Yb)_N$ varies from 1.04 to 7.90. The Bornaward granitoid samples are characterized by low to moderate sum REE contents (44.8–293.5 ppm), with strongly fractionated REE patterns and LREE enrichment compared to HREE and with strong negative anomaly of Eu. The negative Eu anomaly occurs in all of the Bornaward granitoid samples and it is attributed to the minor retention of Eu^{2+} by residual plagioclase. The abundance of REE in the high magnetite-bearing granite, displays considerable variations compared to the pattern of other intrusive rocks. The REE exhibit low fractionation with $(La/Lu)_N = 2–7$ and more fractionation for the light REE (LREE) with $(La/Sm)_N = 2.4–2.6$ compared to heavy REE (HREE) with $(Gd/Lu)_N = 1.05–1.1$. The Bornaward granitoid rocks HREE pattern is relatively flat. The BGC Eu anomalies exhibit a significant negative Eu anomaly with a moderately fractioned LREE pattern characterized by $(La/Lu)_N = 1.07–9.23$, $(La/Sm)_N = 1.25–4$ and $(Gd/Lu)_N = 0.4–1.08$. Only the high magnetite-bearing granite has flat Eu anomaly, because of the low abundance or lack of plagioclase in the residue. Also, the primitive mantle-normalized element patterns (Fig. 8) are homogeneous with marked and uniform negative Ba, Nb, Sr, Eu and Ti anomalies. The Sr and Eu negative anomalies can be explained by plagioclase fractionation, whereas the other negative anomalies appear to be inherited by the petrogenetic process. The patterns exhibit substantial negative Eu anomalies that it can be typical of plagioclase fractionation. In the primitive mantle-normalized element patterns (Fig. 8), the LILE and HFSE display more significant fractionation and also the negative Nb anomaly is less significant. The overall REE abundances of the granitoids of Bornaward area coincide with typical crustal derived granitoids (i.e. La is 20–200 times chondrite, Yb is 8–50 times chondrite), as reported by Holtz (1989) and Williamson et al. (1996).

8. Zircon U–Pb dating

Based on field observation, Muller and Walter (1983) suggested that the Taknar Formation has Precambrian age. We used more accurate zircon U–Pb dating, because of zircon U–Pb dating is the best method for age dating of the very ancient regions that have endured different events for examples: tectonic, alteration, weathering, metamorphism and metasomatism.

Four rock samples were chosen for the zircon U–Pb dating as follows:

- Two sample granites: 1 – The granite without magnetite that belongs to the Taknar mine area (west of the study area).
  2 – The magnetite-bearing granite that belongs to the Bornaward area (east of the study area).
- A sample granodiorite that belongs to the Taknar mine area.
- A sample diorite that belongs to the Bornaward area.

The zircon U–Pb dating was done at Department of Geosciences, University of Arizona, (USA). The measured isotopic ratios, U and Pb concentrations, the zircon U–Pb calculated atomic ratios of the four samples, BKTh-1, BKTh-3, TAK2-8 and TAK1-5 and their ages are given in Table 2.

The calculated isotopic age of the granite sample (BKth-1) is presented in the Tuff Zirc diagram. The zircon samples of the granite (BKTh-1) have 34 analyzed points, 20 points on the cores and 14 points on the rims of the zircons. All of these analyses tend to plot along a well-defined discordia line on the concordia plot (Fig. 11A) with a regressed upper intercept mean age value of 550.41 + 3.21, −4.54 Ma (error in the 2 sigma level). The calculated isotopic age for the diorite sample (BKTh-3) is presented in the Tuff Zirc diagram. The zircons of the diorite sample (BKTh-3) have 41 analyzed points, 14 points on the cores and 27 points on the rims of zircons, giving the mean age value of 551.96 ± 4.32 Ma (error in the 2 sigma level) (Fig. 11B). The calculated isotopic age for granodiorite sample (TAK1-5) is shown in the Tuff Zirc graphics. Based on 32 analyzed points, the mean age value of granodiorite is 540.5 ± 2.9 Ma (error in the 2 sigma level) (Fig. 11C). The results of isotopic calculation of granite sample (TAK2-8) have presented in the TuffZirc graphics. Based on 12 analyzed points on the granite sample, the mean age value of the granite is 550 ± 6.9 Ma (error in the 2 sigma level) (Fig. 11D).

Table 2
Results of U–Pb–Th laser-ablation multicollector ICP mass spectrometry analysis of zircon from the Bornaward and Taknar intrusions.

Analysis	U (ppm)	$^{206}Pb/^{204}Pb$	U/Th	$^{206}Pb/^{207}Pb$	± (%)	$^{207}Pb/^{235}U$	± (%)	$^{206}Pb/^{238}U$	± (%)	Age (Ma)	± (m.y.)
BKTh-1 (Bornaward high Fe_2O_3-granite)											
1-1R	848	248,510	1.4	17.1143	1	0.7181	2.1	0.0891	1.9	550.4	9.8
1-1C	101	1839	1.6	16.3106	7.2	0.7563	7.6	0.0895	2.7	552.4	14.2
1-2R	657	6743	1	17.0331	1	0.7201	1.6	0.089	1.3	549.4	6.8
1-2C	842	7504	0.8	17.0883	2.1	0.6889	3.6	0.0854	3	528.2	15
1-3R	385	47,721	1.2	17.0818	1.1	0.6887	1.9	0.0853	1.5	527.8	7.8
1-3C	717	48,973	1.2	17.0886	0.8	0.7144	1.6	0.0885	1.3	546.9	7
71-4R	72	34,973	2.3	17.1674	7.9	0.731	8.2	0.091	2.3	561.5	12.4
1-4C	135	22,933	1.4	17.5311	3.7	0.6865	4	0.0873	1.5	539.4	8
1-5R	539	56,831	1.4	16.8982	1.1	0.718	1.5	0.088	0.9	543.7	4.9
1-5C	503	13,361	1.6	16.8236	1.8	0.7334	2.6	0.0895	1.8	552.5	9.5
1-6R	468	2337	1.1	16.755	3.5	0.7469	3.8	0.0908	1.4	560	7.6
1-6C	608	66,181	1.2	16.9823	1.9	0.7069	3.1	0.0871	2.5	538.2	12.9
1-7C	747	172,605	1	17.0833	1	0.7232	1.5	0.0896	1.2	553.2	6.1
1-9R	761	177,657	0.8	17.1523	0.7	0.71	1.3	0.0883	1	545.6	5.4
1-9C	932	171,473	0.9	17.1473	0.7	0.7211	1.2	0.0897	1	553.6	5.2
1-10R	594	194,187	0.8	17.0934	1	0.7256	1.4	0.09	1	555.3	5.4
1-10C	523	273,349	1.2	17.2122	1.1	0.7062	1.8	0.0882	1.4	544.7	7.4
1-11R	1024	266,461	0.8	17.1479	0.5	0.7276	1.8	0.0905	1.7	558.4	8.9
1-11C	199	37,370	1.9	17.2089	2.9	0.7029	3.1	0.0877	0.9	542.1	4.9
1-12R	300	42,726	1.5	17.1953	1.8	0.7261	2.7	0.0906	2	558.8	10.8
1-12C	635	29,657	1.1	17.0492	0.8	0.7269	1.7	0.0899	1.5	554.8	8.2
1-13R	450	58,506	1.1	16.9506	1.1	0.7264	2.3	0.0893	2	551.4	10.3
1-13C	821	25,368	1	16.9987	1.1	0.7013	2	0.0865	1.7	534.5	8.7
1-15R	392	35,680	1.5	16.9625	2.1	0.7098	2.5	0.0873	1.3	539.7	6.5
1-16R	342	111,972	1.8	17.0475	1.8	0.7577	3.7	0.0937	3.3	577.3	18.2
1-16C	738	187,358	0.9	17.007	0.8	0.7208	1.7	0.0889	1.5	549.1	7.9
1-17R	728	130,866	1.2	17.017	0.8	0.7469	1.6	0.0922	1.3	568.4	7.3
1-18R	238	54,866	1.9	17.0697	4	0.7384	4.2	0.0914	1.3	563.9	7
1-19R	471	48,819	1.5	17.1977	1.3	0.7098	1.5	0.0885	0.7	546.8	3.8
1-19C	577	67,753	1.3	17.0963	1.2	0.7148	1.7	0.0886	1.2	547.4	6.5
1-20R	1.3	8968	2.4	16.7067	9.2	0.74	9.7	0.0897	3.1	553.5	16.3
1-21R	363	83,909	1.4	17.1515	1.1	0.7367	1.5	0.0916	1	565.2	5.4
1-22R	189	31,627	2.4	17.3242	3.9	0.7033	4	0.0884	1.2	545.9	6.2
1-23R	517	100,475	1.1	16.9984	1.1	0.705	2.8	0.0869	2.5	537.2	13
BKTh-3 (Bornaward diorite)											
3-9C	109	2751	1.1	16.5142	8.5	0.7179	8.9	0.086	2.8	531.7	14.1
3-3R	284	2054	1.5	16.9449	2.1	0.7024	2.3	0.0863	0.8	533.7	4.3
3-4R	301	4449	1.1	17.1132	2.7	0.6956	3	0.0863	1.4	533.8	7.3
3-9R	255	10,405	1.4	16.9391	4.3	0.7032	4.6	0.0864	1.5	534.1	7.5
3-23R	234	5474	1.1	16.2706	5.7	0.7357	5.9	0.0868	1.6	536.7	8.1
3-6C	149	38,756	1.3	16.9442	5.2	0.7067	5.8	0.0868	2.6	536.9	13.4
3-26R	469	24,810	1.3	17.0269	2.6	0.7052	2.7	0.0871	1.1	538.3	5.9
3-14R	283	28,791	1.2	16.8449	2.2	0.7128	2.5	0.0871	1.3	538.3	6.7
3-12C	549	96,292	0.8	16.975	1	0.7098	2.3	0.0874	2	540.1	10.5
3-3C	179	74,935	3.3	17.1937	4.3	0.7012	4.6	0.0874	1.7	540.4	8.8
3-22R	384	92,638	0.9	17.0493	2	0.7025	2.2	0.0875	0.9	540.6	4.7
3-11R	447	2422	0.9	16.7778	5	0.7217	5.2	0.0878	1.5	542.7	7.7
3-7C	208	1960	1.2	17.2494	4.9	0.7049	5.3	0.0882	2.1	544.8	10.9
3-18C	547	2304	0.9	16.8063	3	0.7262	3.2	0.0885	1.1	546.8	5.8
3-21R	167	15,291	1.7	17.0019	2.7	0.7186	3	0.0886	1.3	547.3	7.1
3-24R	232	36,251	1.4	17.0231	2.4	0.7181	2.5	0.0887	0.7	547.6	3.5
3-15R	669	145,495	1	16.9534	0.5	0.7211	1.4	0.0887	1.3	547.6	7
3-8R	321	1714	2.2	16.4025	7.2	0.7475	7.3	0.0889	1.6	549.2	8.4
3-13R	310	73,307	1.2	17.0165	3.3	0.7207	3.4	0.0889	0.9	549.3	4.6
3-8R	466	26,588	5.5	16.9136	2	0.7277	2.3	0.0893	1.1	551.2	5.8
3-21C	219	1953	1.2	16.4227	3.4	0.7502	3.7	0.0894	1.4	551.7	7.2
3-2C	371	104,001	1.6	17.06	1.2	0.7225	1.7	0.0894	1.2	552	6.2
3-19R	160	25,886	1.2	17.4389	4.8	0.7073	5.1	0.0895	1.8	552.3	9.3
3-25R	603	124,153	1.3	17.0702	0.9	0.724	1.3	0.0896	1	553.4	5.1
TAK2-8 (Taknar granite)											
2-8-1C	376	24,213	1.7	16.7772	1.5	0.7202	1.8	0.0876	1	541.5	5.1
2-8-2C	245	18,913	1.7	17.167	3.4	0.7116	3.8	0.0886	1.6	547.2	8.3
2-8-3C	263	20,831	1.8	17.2811	3.3	0.7157	3.4	0.0897	0.9	553.8	4.9
2-8-5C	541	44,610	2	17.2002	1.9	0.7017	2.6	0.0875	1.8	540.9	9.5
2-8-6T	429	37,871	2	17.2354	1.2	0.7309	1.8	0.0914	1.3	563.6	6.8
2-8-7T	497	41,350	1.9	17.2885	1.1	0.7139	2.1	0.0895	1.9	552.7	9.8
2-8-8C	422	21,395	1.7	17.023	1.4	0.6743	1.9	0.0832	1.3	515.5	6.6
2-8-9C	146	54,031	1.9	17.8001	4.7	0.7065	9.9	0.0861	8.7	532.3	44.3
2-8-10C	289	61,030	1.5	16.9	3	0.735	3.4	0.0901	1.6	556	8.4
2-8-12C	725	52,668	1.3	17.0615	1	0.6883	1.3	0.0852	0.9	526.9	4.5

(*continued on next page*)

Table 2 (*continued*)

Analysis	U (ppm)	$^{206}Pb/^{204}Pb$	U/Th	$^{206}Pb/^{207}Pb$	± (%)	$^{207}Pb/^{235}U$	± (%)	$^{206}Pb/^{238}U$	± (%)	Age (Ma)	± (m.y.)
TAK1-5 (Taknar granodiorite)											
1-5-1C	432	45,846	3.4	14.9263	0.8	1.2464	1.7	0.1349	1.5	815.9	11.1
1-5-2C	461	40,369	2.1	16.9605	1.4	0.7346	1.4	0.0904	0.3	557.7	1.8
1-5-3T	305	34,228	2.3	17.3272	2.8	0.6938	2.9	0.0872	0.7	538.9	3.8
1-5-4T	628	21,930	2.8	17.048	1.5	0.6695	1.7	0.0828	0.7	512.7	3.6
1-5-5C	564	99,521	1.1	13.9042	0.6	1.6024	4	0.1616	4	983.7	11.9
1-5-6T	1071	94,482	2.9	16.4676	0.9	0.8479	1.8	0.1013	1.6	621.9	9.6
1-5-7C	448	30,356	3.1	17.0575	1.2	0.6981	1.7	0.0864	1.2	534	6
1-5-8C	360	33,821	3.7	16.8601	1.4	0.7605	4.9	0.093	4.7	573.2	25.7
1-5-9C	1202	112,969	2	17.0753	0.4	0.6973	1.4	0.0864	1.3	533.9	6.7
1-5-10C	529	35,368	3.8	16.9637	0.7	0.6901	1.4	0.0849	1.1	525.3	5.7
1-5-11C	290	21,759	4.1	17.0125	3.2	0.6766	3.4	0.0835	1.3	516.9	6.6
1-5-12T	329	33,909	3.5	17.0886	1.4	0.7222	1.7	0.0895	4	552.6	5.2
1-5-13T	446	42,534	2.6	17.0743	1.3	0.7181	2	0.0889	1.5	549.2	7.8
1-5-14T	938	61,488	2.7	16.8978	0.7	0.7317	2.5	0.0897	2.4	553.6	12.7
1-5-16T	271	15,615	1.7	16.603	4	0.7184	4.9	0.0865	2.8	534.8	14.2
1–5-17T	542	40,302	1.6	16.8853	1.2	0.6911	2.5	0.0846	2.2	523.7	11.3
1-5-18C	510	34,756	1.3	19.9926	1.3	0.7133	1.5	0.0879	0.8	543.2	4.4
1-5-19T	376	30,795	2.1	17.0282	2.2	0.7159	3.9	0.0884	3.2	546.1	16.8
1-5-20T	258	27,504	2.1	17.3455	1.4	0.6987	1.7	0.0879	0.9	543.1	4.7
1-5-21T	400	26,329	3.1	16.7358	2.8	0.7597	3.5	0.0922	2.1	568.6	11.2
1-5-22T	313	23,018	1.6	17.0354	2.3	0.7057	4.8	0.0872	4.2	538.9	21.9
1-5-23T	738	67,172	1.4	17.0728	0.9	0.7057	1.4	0.0874	1.1	540	5.6
1-5-24T	481	53,142	2.4	17.0398	0.9	0.7065	1.6	0.0873	1.3	539.7	6.9
1-5-25T	227	19,898	2.8	16.8117	2.1	0.7082	2.8	0.0864	1.9	533.9	9.7
1-5-27T	335	11,428	3.3	16.633	5.4	0.7209	5.5	0.087	0.7	537.6	3.4
1-5-28T	573	27,325	1.7	16.9589	1.3	0.7047	2.4	0.0867	2	535.8	10.3
1-5-29T	258	31,373	1.9	16.334	1.2	0.892	2.4	0.1057	2.1	647.6	12.6
1-5-30T	613	18,986	1.7	16.8825	1.6	0.7123	2.7	0.0872	2.2	539.1	11.3
1-5-31T	412	35,728	2.9	16.9675	2	0.6992	2.9	0.086	2	532.1	10.3
1-5-32T	421	23,796	4	16.7739	1.5	0.6941	2.4	0.0844	1.9	522.5	9.7

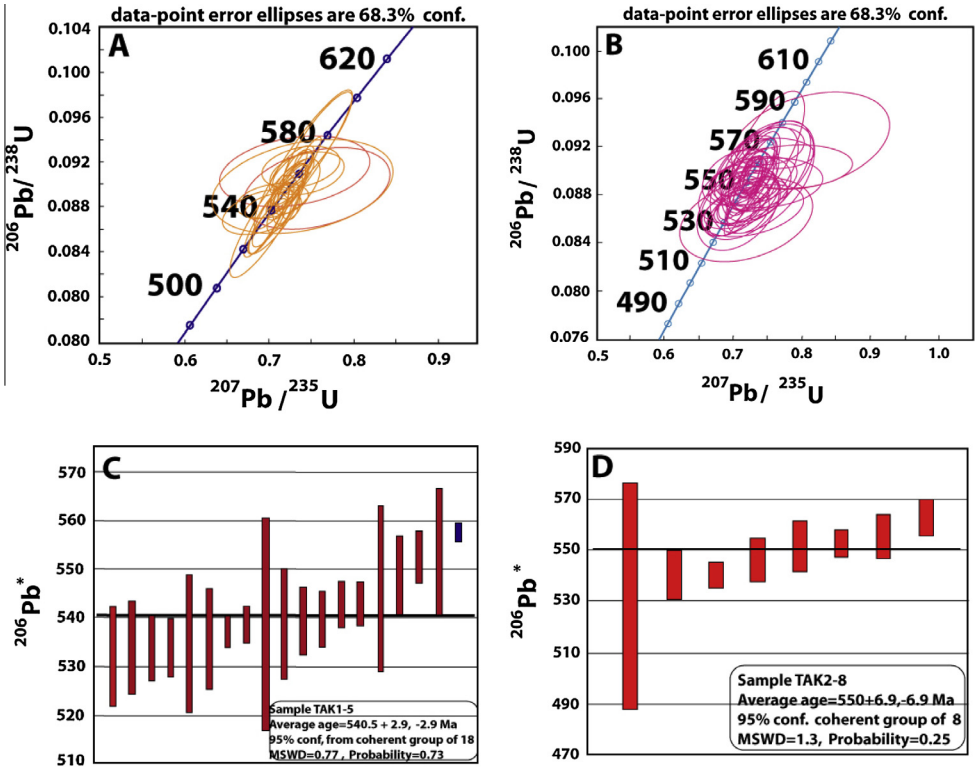

Fig. 11. (A) Zircon U–Pb dating of the Bornaward granite: (a) concordia diagram. (B) Zircon U–Pb dating of the Bornaward diorite: (a) concordia diagram. (C) TuffZirc graphics calculating the age of zircons of the Taknar granite (TAK1-5). (D) TuffZirc graphics for calculating the age of zircons of the Taknar granodiorite (TAK2-8).

The relatively invariable U/Th ratios and their respective spot U–Pb ages (Table 2) are consistent to the magmatic zircons, and no inherited components were detected. These characteristics together with the high closure temperatures of zircon (e.g., Cherniak and Watson, 2000) allow us to interpret the U–Pb data as representation of the crystallization ages of the igneous

protolith(s) of the Bornaward Granitoid. Therefore, the zircon U–Pb dating indicates that all of the four samples are located within the Precambrian (Late NeoProterozoic) time.

9. Sr–Nd isotopes

The Sr and Nd isotope data for representative samples are given in Table 3. They have a range of $(^{87}Sr/^{86}Sr)_i$ and $(^{143}Nd/^{144}Nd)_i$ from 0.703514 to 0.716888 and from 0.511791 to 0.512061, respectively. When these data recalculated to an age of 553 and 538 Ma, they are consistent to the new radiometric results (Table 3). The initial εNd isotope values for the granite, granodiorite, monzogranite and diorite range from −6.73 to 2.52 (Table 3).

10. Discussion

10.1. Source of magma of Bornaward Granitoid Complex

The chemically BGC rocks locate in middle-high metaluminous to slightly-middle peraluminous group (A/CNK = 0.70–1.82). Also, based on SiO_2–K_2O diagram (Peccerillo and Taylor, 1976), the BGC rocks belong to tholeiite, Calc-alkaline and High K-calc-alkaline series. The K enrichment in high-K_2O igneous rocks has been variously interpreted: (1) the K enrichment is due to partial melting of an enriched mantle (Bloomer et al., 1989; Muller and Groves, 1995), (2) magma mixing and crustal contamination (Bachmann and Bergantz, 2008; Mamani et al., 2008), and (3) lower crustal assimilation in MASH (Melting-Assimilation-Storag e-Homogenization) or "Hot Zones" are also postulated to yield high-K_2O igneous rocks (Annen et al., 2006).

Ascent of magmas through thickened continental crust can allow to crustal contamination resulting in higher Rb/Sr and LILE/HFSE ratios and increased K_2O and Th contents due to assimilation and fractional crystallization processes (Esperanca et al., 1992). The studied intrusive rocks display enrichment of LILE (Cs, Rb, Ba, La, Nd, Hf, Zr, Y and U) and LREE (La and Sm), depletion of HFSE (Nb, Ta, Sr and Ti) and HREE (Gd and Lu), and negative Eu anomalies.

The Ti, Nb and Ta negative anomalies (Fig. 7) are typical of all types of calc-alkaline magmas and may be explained by residual hornblende and/or Fe–Ti oxides (rutile, ilmenite) in the source of the parental magmas (Martin, 1999).

Phosphorous exhibits negative anomalies in the studied samples which may be related to apatite fractionation. Decreasing P_2O_5 and CaO values with increasing SiO_2 in the Harker diagram also support apatite fractionation. However, the trend of incompatible elements such as alkaline elements ($Na_2O + K_2O$) and Yb vs. SiO_2 is ascending. The variations in major and trace elements of the BGC show the normal partial crystallization trend of hornblende, biotite, plagioclase and titanomagnetite, and the accumulation of incompatible elements in the rest of magma.

In agreement with the high metaluminous to middle peraluminous and S-type characteristics already noted for the intrusive rocks, rocks show that the BGC rocks plot in the field of the volcanic arc granites in the diagrams proposed by Pearce et al. (1984) (Fig. 12). Location of some of the Bornaward Granitoid Complex rocks in WPG and ORG fields is because of intense metamorphism, alteration and tectonic effects on the rocks after magmatism (Termal et al., 1998; Pearce, 1983).

The compositions of Bornaward granitoid rocks have plotted on the CaO/Na_2O–Al_2O_3/TiO_2 diagram (Fig. 13). The field of S-type granitoids and its boundaries has separated from other granitoids (Sylvester, 1998). Some of the BGC rocks with low SiO_2 content (<71 wt.%), have high FeOt + MgO + TiO_2 (>4 wt.%) and high CaO/Na_2O ratios, but the BGC rocks with high SiO_2 (>71 wt.%), have

Table 3
Rb–Sr and Sm–Nd isotopic compositions of the Bornaward and Taknar intrusions.

Sample	Rb (ppm)	Sr (ppm)	Sm (ppm)	Nd (ppm)	$^{87}Rb/^{86}Sr$	$(^{87}Sr/^{86}Sr)_m$ (2σ)	$(^{87}Sr/^{86}Sr)_i$	$^{147}Sm/^{144}Nd$	$(^{143}Nd/^{144}Nd)_m$ (2σ)	$(^{143}Nd/^{144}Nd)_i$	εNdi	T_{DM}	U–Pb zircon age (Ma)
BKTh-1	81.7	105	13.52	53.1	2.24	0.721114 ± 0.000010	0.70351	0.1539	0.512374 ± 0.000120	0.511819	−2.1	1.7	550
BKTh-3	46.2	108	8.393	33.319	1.24	0.713477 ± 0.000009	0.70378	0.1524	0.512608 ± 0.000032	0.512061	2.5	1.08	552
BKCh-6	85	122.2	12.23	47.5	2.01	0.721051 ± 0.000016	0.70525	0.156	0.512408 ± 0.000012	0.511847	−1.6	1.62	550
BKCh-8	51.5	30.4	6.99	28.4	4.92	0.744373 ± 0.000019	0.7058	0.149	0.512312 ± 0.000015	0.511776	−3	1.66	550
BKCh-15	100	229	6.22	31.4	1.26	0.719132 ± 0.000022	0.70921	0.12	0.512017 ± 0.000014	0.511585	−6.7	1.63	550
TK1-5	111	50	6.18	27	6.02	0.766090 ± 0.000009	0.71689	0.1385	0.512330 ± 0.000032	0.511842	−2	1.44	538
TK2-8	41	79	7.7	36	1.5	0.725390 ± 0.000010	0.71356	0.1294	0.512260 ± 0.000120	0.511791	−2.6	1.41	553

m = measured. Errors are reported as 2σ (95% confidence limit). $(^{143}Sr/^{144}Sr)_i$ is the initial ratio of $^{87}Sr/^{86}Sr$ for each sample, calculated using $^{87}Rb/^{86}Sr$ and $(^{87}Sr/^{86}Sr)_m$ and an age of 538–553 for intrusive rocks. $(^{87}Nd/^{86}Nd)_i$ is the initial ratio of $^{143}Nd/^{144}Nd$ for each sample, calculated using $^{147}Sm/^{144}Nd$ and $(^{143}Nd/^{144}Nd)_m$ and an age of 538–553 for intrusive rocks. $εNd_i$ is initial εNd value.

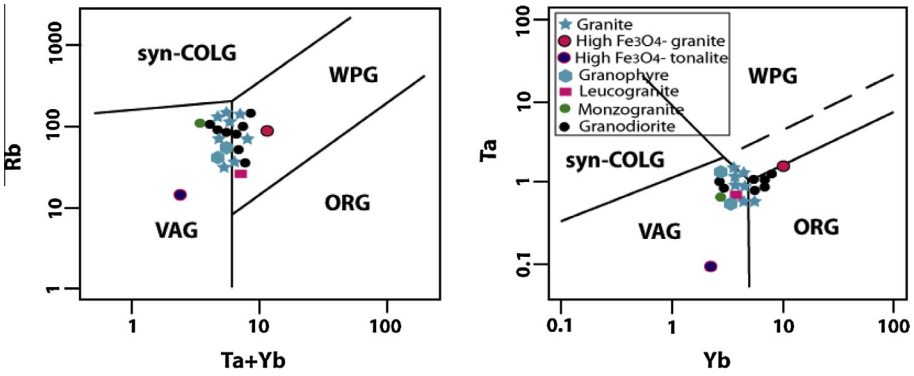

Fig. 12. Tectonomagmatic discrimination diagrams for the Bornaward intrusive rocks (after Pearce et al., 1984). WPG: within-plate granitoids; VAG: volcanic arc granitoids; ORG: ocean ridge granitoids; syn-COLG: syncollisional ranitoids.

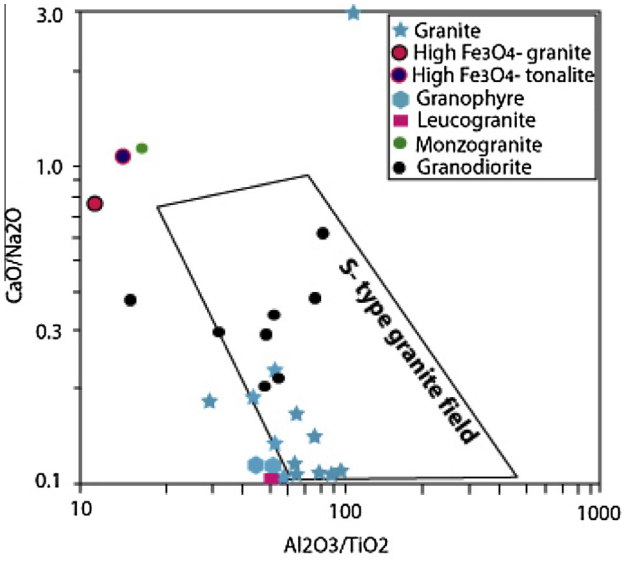

Fig. 13. Compositions of granitic rocks from the Bornaward plotted on the CaO/Na_2O–Al_2O_3/TiO_2 diagram. The field of S-granites and its boundaries types. The Bornaward granitoids are plotted in the field of S –type granite.

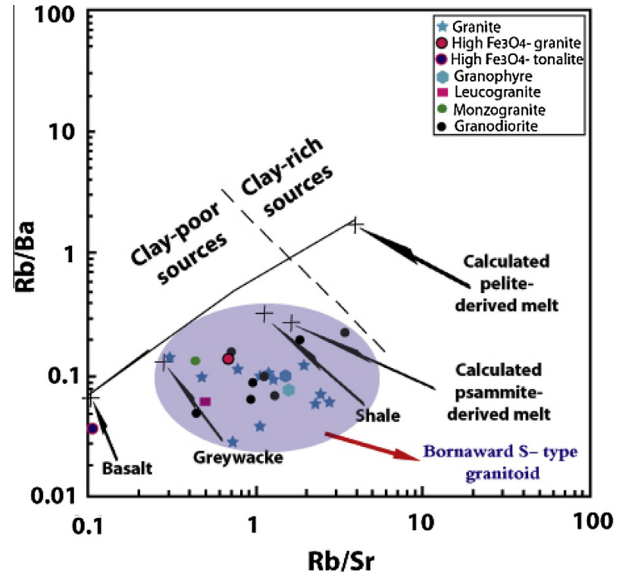

Fig. 14. Plot of Rb/Sr vs. Rb/Ba, the melt of Bornaward S-type granitoids derived psammite and greywacke rocks.

low FeOt + MgO + TiO_2 (<4 wt.%) and low CaO/Na_2O ratios. Most of the BGC rocks locate in the S-type granite field. These relationships are consistent with the low CaO/Na_2O S-granites having pelitic sources and consistent with high CaO/Na_2O S-granites having psammitic sources (Sylvester, 1998).

It is certainly true that production of most granites (and especially S-types) has involved the partial melting of crustal rocks. Thus, granites are dominantly the products of crustal recycling, rather than juvenile crustal additions (Clemens, 2003).

The Rb/Sr vs. Rb/Ba diagram shows the Bornaward Granitoid bodies plot next to metapsammite and metagreywacke derived melts (Fig. 14). Because Sr and Ba are compatible in plagioclase, whereas Rb is incompatible (e.g., Harris and Inger, 1992), psammite-derived melts will tend to have higher Rb/Sr and Rb/Ba than their sources. Thus, Rb/Sr and Rb/Ba of S-type granite melts are a function not only of the source composition but also the amounts of plagioclase and K-feldspar left behind in the source region. Psammitic rocks, particularly meta-greywackes, are widespread at convergent plate margins and are thus likely to have been available for anatexis in many crustal blocks accreted in collisional zones (Vielzeuf and Montel, 1994). The predominance of pelite or psammite sources of S-granites in a particular collision belt may reflect the maturity of the accreted crustal blocks, with psammite sources pointing to immature plate margin successions. In general, the melt produced at low melting fractions is indistinguishable (mainly metaluminous), irrespective of the nature of the protolith. Metaluminous meta-igneous rocks are able to produce peraluminous felsic melts at low melting fractions and in water-deficient conditions (Sylvester, 1998; Karimpour et al., 2010).

The initial $^{87}Sr/^{86}Sr$, $^{143}Nd/^{144}Nd$ and εNd of the Bornaward and Taknar mine intrusive rocks (Table 3) have plotted in Fig. 15. The Bornaward area has located in 7 km east of the Taknar mine area. The initial $^{87}Sr/^{86}Sr$ isotope values for the BGC rocks range from 0.70351 to 0.70921, for the Taknar intrusive rocks range from 0.71356 to 0.71688 and MORB is less than 0.7040. The initial $^{143}Nd/^{144}Nd$ isotope values for the Bornaward intrusive rocks range from 0.511585 to 0.512061 and for the Taknar mine intrusive rocks range from 0.511791 to 0.511842. This indicates the source of magma for both the Bornaward and Taknar granitoids originated from the lower and upper continental crust and source of magma for the Taknar intrusive rocks was more radiogenic.

Samarium–Neodymium T_{DM}'s can provide an estimate for the time at which contamination of continental crust was extracted from a depleted mantle source. Therefore, T_{DM} ages may delineate crustal blocks of differing ages. The BGC yields a T_{DM} age of 1.08–1.70 Ga. This indicates that the intrusive rocks have been derived from partial melting of distinct basement source regions. The

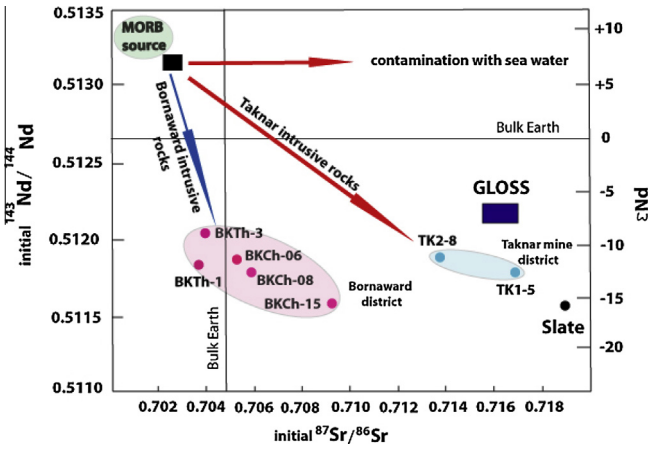

Fig. 15. A $^{143}Nd/^{144}Nd$–$^{87}Sr/^{86}Sr$ diagram for the Bornaward intrusive rocks for $T = 0$ Ma. This shows that the change in $^{87}Sr/^{86}Sr$ ratios is not related to an alteration caused by seawater, and further implies a mixing of source magma with subduction sediments (Rollinson, 2007), since seawater would not significantly change the Nd-isotope ratio. The trend seen in the metabasites is similar to the volcanic rocks island arc and infers the mixing of source magma with slab sediments. GLOSS is the average composition of global subducting sediment from Plank and Langmuir (1998).

values of initial εNd suggest that the intrusive rocks of Taknar mine district originated from a depleted mantle. In the Nd–Sr isotope diagram (Rollinson, 1993), all of the BGC rocks show a negative correlation between the Nd and Sr ratios (Fig. 15).

In following of the collision of the Iranian and Turan plates, crustal shortening and thickening occurred. In continental collision zones, thickening of continental crust allows melting of metapsammite, metagreywackes, and meta-igneous rocks under hydrated conditions. Such melting can produce silicic to intermediate-composition magmas of different series (i.e.; Petford and Atherton, 1996). However, the initial $^{87}Sr/^{86}Sr$ values of the BKTh-1, BKTh-3, BKCh-06 and BKCh-08 in the Bornaward district (0.70351–0.70921) are different from the value shown by the slate (0.71931). This difference indicates that although the source of the magma was in continental crust, the source was not solely the slate-related rock types. Whereas, the initial $^{87}Sr/^{86}Sr$ values of the TK2-8 and TK1-5 in the Taknar district (0.71356 and 0.71689) are near to slate.

10.2. Distribution of Late Neoproterozoic granitoids in Iran plate

During and after the Katangan orogeny phase was created folding and deep fractures in Iran Continental Crust (basement). The

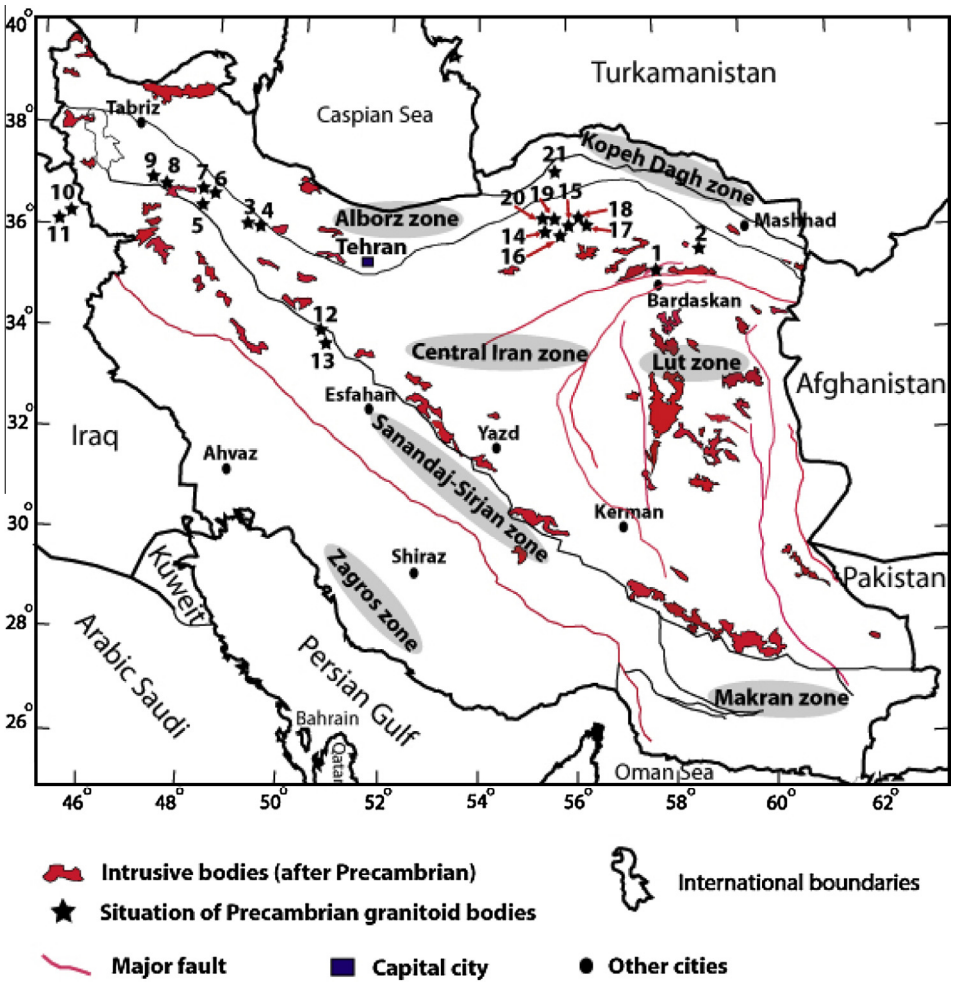

Fig. 16. Distribution of Late Neoproterozoic igneous plutons in Iran (provided by Reza Monazzami Bagherzadeh and adapted from data of Hassanzadeh et al., 2008, with additions), 1 – Bornaward granite, granodiorite and diorite, 2 – Arghash diorite, 3 & 4 – Sarv-e Jahan leucogranite and biotite granite, 5 – Khorram Darreh biotite granite, 6 – Doran leucogranite, 7 – West of Doran leucogranite, 8 – Moghanlou biotite granite mylonite, 9 – Mahneshan biotite granite mylonite, 10 – Bubaktan biotite granite, 11 – Sheikh Chupan biotite granodiorite, 12 – Chah Khatoon biotite leucogranite, 13 – North Varzaneh biotite granite mylonite, 14 – Shotor Kuh, NE of Torud biotite granite mylonite, 15 – Kuh-e Molhedou leucogranite, 16 – Kuh-e Sefid Sang biotite granite, 17 – Delbar, SE Kuh-e Molhedou leucogranite, 18 – Kuh-e Molhedou Biotite-garnet granite, 19 & 20 – Band-e Hezar Chah leucogranite and leucogranite mylonite, 21 – Leila Kuh, SW Langarud Pink biotite granite.

result of this process was appearance of alkalin magmas in Infracambrian and Paleozoic time in many parts of Iran either intrusive bodies (for example: Bornaward Granitoid Complex) or alkalin volcanic bodies (for example: Taknar alkalin rhyolite). All of these signs indicate expansion of Iran Continental Crust and creation of rift. At this time, horsts and grabens were created and microcontinentals become separated.

The Bornaward Granitoid Complex of exposed in the northeast of Central Iran has Late Neoproterozoic age. Distribution of Late Neoproterozoic igneous plutons in Iran ranging in age from 599 to 544 Ma are widespread across Central Iran and the Sanandaj–Sirjan structural zone (Fig. 16 – adapted from data of Hassanzadeh et al., 2008, with additions). This data have provided on the basis of zircon U–Pb dating. They are dominantly felsic in composition but a few intermediate to mafic plutons are also present.

11. Conclusions

Based on zircon U–Pb dating, the oldest of Iran granitoid bodies have formed into older metamorphosed rocks in the Late Neopro terozoic–Cambrian. Most of Late Neoproterozoic (Precambrian) granitoids have located in the Central Iranian Block. The Bornaward Granitoid Complex (BGC) is one of the oldest magmatic intrusions exposed in the Taknar Zone that belong to the Central Iranian Block and represent the elements of a terminal Late Neoproterozoic–Early Cambrian magmatic arc complex.

Chemically, the Bornaward Granitoid rocks are middle-high metaluminous to low-middle peraluminous and belong to Tholeiite, Calc-alkaline to high-K calc-alkaline series with enrichment in LILE = Cs, Rb and Ba, K, Zr, Y, Th, U, La and Hf elements and depletion in HILE = Sr and Nb, Ta, Ti elements. Based on K_2O enrichment, the BGC rocks belong to high-K calc alkaline series and a clear enrichment in large-ion lithophile elements (LILE) coupled with high-field-strength elements (HFSE) depletion, with Nb, Ta and Ti negative anomalies.

Mineral composition, and geochemical signature of the Bornaward Granitoid Complex rocks are consistent with origin and source of partial melting of continental crust to produce S-type intrusive rocks.

The results of zircon U–Pb dating for two granites (BKTh-1 and TK2-8 samples) are 550.41 + 3.21, −4.54 and 540.5 ± 2.9 Ma, respectively. Also, the zircon U–Pb dating of the granodiorite (TK1-5 sample) and diorite (BKTh-3 sample) are 550.6 ± 6.9 and 551.96 ± 4.32, respectively. The ages of these rocks belong to Precambrian (Late Neoproterozoic time). Also, they have the initial $^{87}Sr/^{86}Sr$ and $^{143}Nd/^{144}Nd$ values ranging from 0.70351 to 0.716888 and 0.511585 to 0.512601, respectively. The initial εNd isotope values for granites, granodiorite, monzogranite and diorite range from −6.73 to 2.52. T_{DM} age of the BGC is 1.08–1.70 Ga. This indicates that the Bornaward intrusive rocks have derived from partial melting of distinct basement source regions with very high initial $^{87}Sr/^{86}Sr$ that have undergone extensive crustal contamination.

Presence of rich mica-bearing enclaves (acidic type) are a good evidence related to continental crust to produce magma, while the existence of dark color and fine grain enclaves (basic type) are more an index of related to produced magma from mantle. Also, the enclaves that have irregular and chilled margins, usually appear near of mixing point.

The S-type granites commonly contain fine-grained, igneous-textured enclaves that are more mafic than their host rocks. These are usually interpreted as globules of a separate magma, mingled with the volumetrically dominant host magma (Phillips et al., 1981).

Breaking of plagioclase and quartz crystals and undulatory extinction, having ridged margins and presence of subgrains around coarse grains (recrystallization) in the Bornaward granitoid rocks are signs of event of dynamic and tectonic pressures. Also, creation of fine-grained quartz around coarse grains of quartz indicate two-stage cooling of magma as a result of tectonic events. The subject shows that coarse grains of quartz were crystallized in the first stage and then with a quick movement of magma upward and rapid cooling of it, granules were formed in the second stage. These petrographic events and moreover, micrographic texture in the Bornaward acidic intrusive rocks are indicative of intrusion of magma near the surface (“shallow intrusion”).

Crustal doubling, by thrusting or homogeneous thickening, likewise fails to provide sufficient heat (e.g., England and Thompson, 1984). Generally, we must look to the mantle as a source for the extra heat required. This might be provided through mantle upwelling and crustal thinning, and possibly through the intra- and underplating of mafic magmas. Worldwide, there does seem to be a common temporal and spatial association between major granitic plutonism and crustal extension (post- or anorogenic). Extension and granitic plutonism are linked in some collisional tectonic settings such as Andean margins (e.g., Atherton, 1990), and certainly in eastern Australia (e.g., Allen et al., 1998). Thermal modelling has shown that certain styles of mafic intraplating could be highly efficient in transferring heat into the surrounding crust, to cause partial melting (e.g., periodic multiple sheet injection; Petford and Gallagher, 2001).

Acknowledgements

This research was supported by Ferdowsi University of Mashhad, Iran. The isotope analyses at the University of Aveiro were financially supported by the Geobiotec Research Unit (funded by the Portuguese Foundation for Science and Technology, through project PEst-C/CTE/UI4035/2011). George E. Gehrels and Victor Valencia from Department of Geosciences University of Arizona Tucson achieved the zircon U–Pb dating. Special thanks to Emily Verplanck (Department of Geological Sciences at CU Boulder) and Sara Ribeiro (Laboratorio de Geologia Isotopica da Universidade de Aveiro) for their help in obtaining the isotopic data for this study. Special thanks to Jamal Rowshanravan, Head of Geological Survey and Mining Exploration (North-East Territory) of Iran for his helps in accomplishment of this research.

References

Alavi, M., 1991. Tectonic Map of the Middle East: Tehran. Geological Survey of Iran, Scale 1:5,000,000.
Allen, C.M., Williams, I.S., Stephens, C.J., Fielding, C.R., 1998. Granite genesis and basin formation in an extensional setting: the magmatic history of the northernmost New England Orogen. Aust. J. Earth Sci. 45, 875–888.
Annen, C., Blundy, J.D., Sparks, R.S.J., 2006. The genesis of calcalkaline intermediate and silicic magmas in deep crustal hot zones. J. Petrol. 47, 505–539.
Atherton, M.P., 1990. The Coastal Batholith of Peru: the product of rapid recycling of ‘new’ crust formed within rifted continental margin. Geol. J. 25, 337–350.
Bachmann, O., Bergantz, G.W., 2008. Rhyolites and their source mushes across tectonic settings. J. Petrol. 49, 2277–2285.
Bloomer, S.H., Stern, R.J., Fisk, E., Geschwind, C.H., 1989. Shoshonitic volcanism in the Northern Mariana arc: 1. Mineralogic and major and trace element characteristics. J. Geophys. Res. 94, 4469–4496.
Boynton, W.V., 1984. Geochemistry of the rare earth elements: meteorite studies. In: Henderson, P. (Ed.), Rare Earth Element Geochemistry. Elsevier, Amsterdam, pp. 63–114.
Chappell, B.W., 1999. Aluminium saturation in I- and S-type granites and the characterization of fractionated haplogranites. Lithos 46, 535–551.
Chappell, B.W., White, A.J.R., 1992. I- and S-type granites in the Lachlan Fold Belt. Trans. R. Soc. Edinburgh: Earth Sci. 83, 1–26.
Chappell, B., White, A., 2001. Two contrasting granite types: 25 years later. Aust. J. Earth Sci. 48, 489–499.
Chen, R.X., Zheng, Y.F., Zhao, Z.F., Tang, J., Wu, F.Y., Liu, X.M., 2007. Zircon U–Pb age and Hf isotope evidence for contrasting origin of bimodal protoliths for ultrahigh-pressure metamorphic rocks from the Chinese Continental Scientific Drilling Project. J. Metamorph. Geol. 25, 873–894.
Cherniak, D.J., Watson, E.B., 2000. Pb diffusion in zircon. Chem. Geol. 172, 5–24.

Clemens, J.D., 2003. S-type granitic magmas-petrogenetic issues, models and evidence. Earth Sci. Rev. 61, 1–18.
Crawford, A.R., 1972. Iran, continental drift and plate tectonics. In: 24th International Geological Congress Report of the Session 24, No. 3, pp. 106–112.
Crawford, A.R., 1977. A summary of isotopic age data for Iran, Pakistan and India. Memoire Hors Ser. – Soc. Geol. France 8, 251–260.
England, P., Thompson, A.B., 1984. Pressure–temperature–time paths of regional metamorphism: part I. Heat transfer during the evolution of regions of thickened continental crust. J. Petrol. 25, 894–928.
Esperanca, S., Crisci, M., de Rosa, R., Mazzuli, R., 1992. The role of the crust in the magmatic evolution of the island Lipari (Aeolian Islands, Italy). Contrib. Miner. Petrol. 112, 450–462.
Fuping, P., Wenliang, X., Debin, Y., Quanguo, Z., Xiaoming, L., Zhaochu, H., 2007. Zircon U–Pb geochronology of basement metamorphic rocks in the Songliao Basin. Chin. Sci. Bull. 52, 942–948.
Gehrels, G.E., Valencia, V.A., Ruiz, J., 2008. Enhanced precision, accuracy, efficiency, and spatial resolution of U–Pb ages by laser ablation–multicollector-inductively coupled plasma-mass spectrometry. Geochem. Geophys. Geosyst. 9 (3), 1–13.
Ghalamghash, J., Nédélec, A., Bellon, H., Vousoughi-Abedini, M., Bouchez, J.L., 2009. The Urumieh plutonic complex: a magmatic record of the geodynamic evolution of the Sanandaj-Sirjan zone (NW Iran) during Cretaceous times – part II: petrogenesis and $^{40}K/^{40}Ar$ dating. J. Asian Earth Sci. 5, 401–415.
Ghoorchi, M., 2004. Geology, Mineralogy and Geochemistry of Taknar Deposit (Tak-III & IV), Bardaskan. M.Sc. Thesis, Ferdowsi University of Mashhad, 219 p.
Gribble, C.D., 1988. Rutley's Elements of Mineralogy, 27th ed. Unwin Hyman, London.
Gromet, L.P., Silver, L.T., 1987. REE variations across the Peninsular Ranges Batholith: implications for batholithic petrogenesis and crustal growth in magmatic arcs. J. Petrol. 28, 75–125.
Harris, N.B.W., Inger, S., 1992. Trace element modelling of pelite-derived granites. Contrib. Miner. Petrol. 110, 46–56.
Harrison, T.N., 1990. Chemical variation in micas from the Cairngorm pluton, Scotland. Mineral. Mag. 54, 355–366.
Hassanipak, A.A., Ghazi, M., 2000. Petrology, geochemistry and tectonic setting of the Khoy ophiolite, northwest Iran: implications for Tethyan tectonics. J. Asian Earth Sci. 18, 109–121.
Hassanzadeh, J., Stockli, D.F., Horton, B.K., Axen, G.J., Stockli, L.D., Grove, M., Schmitt, A.K., 2008. U–Pb zircon geochronology of Late Neoproterozoic–Early Cambrian granitoids in Iran: implications for paleogeography, magmatism, and exhumation history of Iranian basement. Tectonophysics 451, 71–96.
Holtz, F., 1989. Importance of melt fraction and source rock composition in crustal genesis – the example of two granitic suites of northern Portugal. Lithos 24, 21–35.
Huckriede, R., Kürsten, M., Venzlaff, H., 1962. Zur geologie des gebiets zwischen Kerman und Saghand (Iran). Beihefte zum Geol.- chen Jahrbuch 51, 197.
Karimpour, M.H., Stern, C.R., Farmer, G.L., 2010. Zircon U–Pb geochronology, Sr–Nd isotope analyses, and petrogenetic study of the Dehnow diorite and Kuhsangi granodiorite (Paleo-Tethys), NE Iran. J. Asian Earth Sci. 37, 384–393.
Khalatbari-Jafari, M., Juteau, T., Bellon, H., Emami, H., 2003. Discovery of Two Ophiolite Complexes of Different Ages in the Khoy Area (NW Iran). CR Geosciences 335. Académie des Sciences, Paris, pp. 917–929.
Ludwig, K.R., 2003. ISOPLOT 3.0: A Geochronological Toolkit for Microsoft Excel. Special Publication No. 4. Berkeley Geochronology Center, California, p. 70.
Malekzadeh Shafaroudi, A., 2004. Geology, Mineralogy and Geochemistry of Taknar Polymetal (Cu–Zn–Au–Ag–Pb) Deposit (Tak-I & II) and Determining Type of Mineralization. M.Sc. Thesis, Ferdowsi University of Mashhad, 287p.
Mamani, M., Worner, G., Thouret, J.C., 2008. Tracing a major crustal domain boundary based on the geochemistry of minor volcanic centers in southern Peru. In: 7th International Symposium on Andean Geodynamics (ISAG 2008, Nice), Extended Abstracts, pp. 298–301.
Maniar, P.D., Piccoli, P.M., 1989. Tectonic discrimination of granitoids. Geol. Soc. Am. Bull. 101, 635–643.
Martin, H., 1999. The adakitic magmas: modern analogues of Archean granitoids. Lithos 46 (3), 411–429.
Masoudi, F., Yardley, B.W.D., Clif, R.A., 2002. Rb–Sr geochronology of pegmatites, plutonic rocks and a hornfels in the region south-west of Arak, Iran. J. Sci. Islamic Republ. Iran 13, 249–254.
McDonough, W.F., Sun, S.S., 1995. The composition of the Earth. Chem. Geol. 120, 223–253.
Middlemost Eric, A.K., 1994. Naming materials in the magma igneous rock system. Earth Sci. Rev. 37 (3–4), 215–224.
Muller, D., Groves, D.I., 1995. Potassic Igneous Rocks and Associated Gold-Copper Mineralization. Springer-Verlag, Berlin.
Muller, R., Walter, R., 1983. Geology of the Precambrian–Paleozoic Taknar Inliers Northwest of Kashmar, Khorasan Province, NE Iran. GSI Reports. No. 51, pp. 165–183.
Pearce, J.A., 1983. Role of the sub-continental lithosphere in magma genesis at active continental margins. In: Hawkesworth, C.J., Norry, M.J. (Eds.), Continental Basalts and Mantle Xenoliths. Shiva, Nantwich, pp. 230–249.
Peccerillo, A., Taylor, S.R., 1976. Geochemistry of Eocene calc-alkaline volcanic rocks from the Kastamonu area, Northern Turkey. Contrib. Miner. Petrol. 58, 63–81.
Petford, N., Atherton, M., 1996. Na-rich partial melts from newly underplated basaltic crust: the Cordillera Blanca Batholith, Peru. J. Petrol. 37, 1491–1521.
Petford, N., Gallagher, K., 2001. Partial melting of mafic (amphibolitic) lower crust by periodic influx of basaltic magma. Earth Planet. Sci. Lett. 193, 483–499.
Phillips, G.N., Wall, V.J., Clemens, J.D., 1981. Petrology of the Strathbogie batholith: a cordierite-bearing granite. Can. Mineral. 19, 47–64.
Rollinson, H.R., 1993. Using Geochemical Data: Evaluation, Presentation & Interpretation. Longman Group, UK Ltd., Co-published in the United States with John Wiley and Sons, New York, pp. 352.
Soltani, A., 2000. Geochemistry and Geochronology of I-type Granitoid Rocks in the Northeastern Central Iran Plate. PhD Thesis, University of Wollongong, Australia, 300 p.
Stöcklin, J., 1968. Structural history and tectonics of Iran: a review. Am. Assoc. Pet. Geol. Bull. 52, 1229–1258.
Stöcklin, J., 1974. Possible ancient continental margins in Iran. In: Burk, C.A., Drake, C.L. (Eds.), The Geology of Continental Argins. Springer Verlag, New York, pp. 873–887.
Stöcklin, J., Nabavi, M., 1972. Tectonic Map of Iran. Geological Survey of Iran.
Sun, S.S., McDonough, W.F., 1989. Chemical and isotopy systematics of oceanic basalts: implications for mantle composition and processes. In: Magmatism in the Ocean: Basins. The Geological Society of London Special Publication 42.
Sylvester, P.J., 1998. Post-collisional strongly peraluminous granites. Lithos 45, 29–44.
Taylor, S.R., McLennan, S.M., 1995. The geochemical evolution of the continental crust. Rev. Geophys. 33, 241–265.
Termal, A., Gundogdu, M.N., Gourgaud, A., 1998. Petrological and geochemical characteristics of Cenozoic high-K calc-alkaline volcanism in Konya, Central Anatolia, Turkey. J. Volcanol. Geotherm. Res. 85, 327–354.
Vielzeuf, D., Montel, J.M., 1994. Partial melting of metagreywackes: I. Fluid-absent experiments and phase relationships. Contrib. Miner. Petrol. 117, 375–393.
Whalen, J.B., Currie, K.L., Chappell, B.W., 1987. A-type granites: geochemical characteristics, discrimination and Petrogenesis. Contrib. Miner. Petrol. 95, 407–419.
Williamson, B.J., Shaw, A., Downes, H., Thirlwall, M.F., 1996. Geochemical constraints on the genesis of Hercynian two-mica leucogranites from the Massif Central, France. Chem. Geol. 127, 25–42.
Wyborn, D., 1983. Fractionation Processes in the Boggy Plain Zoned Pluton. PhD Thesis, Australian National University, Canberra.